

**Boron Dipyrromethene (BODIPY) in Polymer Chemistry**

Journal:	<i>Polymer Chemistry</i>
Manuscript ID	PY-REV-10-2020-001513.R1
Article Type:	Review Article
Date Submitted by the Author:	25-Nov-2020
Complete List of Authors:	Lu, Pengtao; The University of Texas at Austin, Chemistry Chung, Kun-You; The University of Texas at Austin, Chemistry Stafford, Alex; The University of Texas at Austin, Chemistry Kiker, Meghan; The University of Texas at Austin, Chemistry Kafle, Kristina; The University of Texas at Austin, Chemistry Page, Zachariah; The University of Texas at Austin, Chemistry

## ARTICLE

## Boron Dipyrromethene (BODIPY) in Polymer Chemistry

Pengtao Lu,<sup>#a</sup> Kun-You Chung,<sup>#a</sup> Alex Stafford,<sup>a</sup> Meghan Kiker,<sup>a</sup> Kristina Kafle<sup>a</sup> and Zachariah A. Page<sup>\*a</sup>

Received 00th January 20xx,  
Accepted 00th January 20xx

DOI: 10.1039/x0xx00000x

Boron dipyrromethenes (BODIPYs) are versatile dyes with diverse structures and associated optoelectronic properties. Their integration into soft materials (polymers) has enabled a myriad of applications from biological/environmental (e.g., imaging, sensing, and therapy) to organic electronic devices and synthesis/degradation. The story herein is meant to guide the reader from the bottom-up, starting with general syntheses of BODIPYs, followed by a discussion of photophysical and electrochemical properties as they relate to structure. These structure-property relationships are then connected to three light driven transformations that are central to the utility of BODIPYs in materials science: 1) electron/energy transfer; 2) triplet formation, and 3) photolysis. Next, the synthetic integration of BODIPYs as structural motifs in both  $\pi$ -conjugated and non- $\pi$ -conjugated polymers is described, along with prescribed methods to tailor their optoelectronic properties. These properties are then correlated to recent utility of BODIPYs within polymer science, both fundamental – examination of polymer dynamics and self-assembly – and applied – biomedicine, optoelectronics, chemosensors, small molecule photoredox catalysis, and photo-polymerization and -degradation. The end of this review provides a summary of the rich history and outlook on the exciting future opportunities for this burgeoning field of BODIPYs in polymer chemistry.

### 1. Introduction

Boron dipyrromethenes (BODIPYs) were prepared serendipitously by Treibs and Kreuzer in 1968 as they were attempting to synthesize an acylated pyrrole from dimethylpyrrole with acetic anhydride using  $\text{BF}_3 \cdot \text{OEt}_2$  as a Lewis acid.<sup>1</sup> Since the discovery, BODIPYs have found applications in a myriad of areas from imaging and therapy to organic electronics and synthesis.<sup>2–15</sup> In a seemingly disparate vein, nearly fifty years prior represents the celebrated birth of polymer science, when Hermann Staudinger raised up his “macromolecular hypothesis” in 1920.<sup>16,17</sup> Now, after 100 years, both natural and synthetic polymer materials have become indispensable and ubiquitous in modern society, ranging from their utility in food packaging to fabrics for spacecraft composites.<sup>18–22</sup> It was thus inevitable that polymers and BODIPYs would be integrated to combine attractive macromolecular (e.g., biocompatibility and processability) and optoelectronic (e.g., luminescence and redox) properties intrinsic to each, respectively. Systematic structural variations to BODIPYs has enabled fine-tuning of photophysical and electrochemical properties, which has furthered their utility in polymer science as dyes for fluorescence imaging of natural macromolecules, such as protein and DNA, as charge transporting units in electronic devices, such as transistors and solar cells, and as light triggered catalysts for the on-demand preparation and degradation of

polymers. To harness the beneficial properties of BODIPYs most efficiently in polymer science, it requires a thorough understanding of structure-property relationships. Thus, in order to accelerate research in this exciting field, we present an overview of BODIPYs in polymer science, a tutorial of sorts, to clearly connect how compositional motifs relate to their utility in both recent and emerging applications.

### 2. Synthesis, Optoelectronic Properties, and Reactivity of BODIPYs

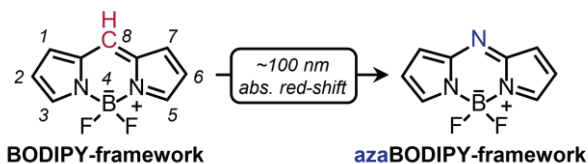
This section focuses on how to select BODIPYs with desired properties. The synthetic routes to access well-known (aza)BODIPY derivatives are reviewed first (section 2.1). Thanks to contributions from synthetic organic chemists, there have been assorted methods to prepare BODIPYs with various functional groups on its framework. We next examine substituent effects on both photophysical and electrochemical properties of functional BODIPYs, intending to help readers understand the underlying structure-property relationships (section 2.2). Finally, three common light-driven (photochemical) reactions for BODIPYs, including electron/energy transfer, triplet formation, and photolysis are described (section 2.3).

<sup>a</sup> Department of Chemistry, The University of Texas at Austin, Austin, Texas 78712, USA.

<sup>#</sup> These two authors contributed equally.

<sup>†</sup> Footnotes relating to the title and/or authors should appear here.

Electronic Supplementary Information (ESI) available: [details of any supplementary information available should be included here]. See DOI: 10.1039/x0xx00000x

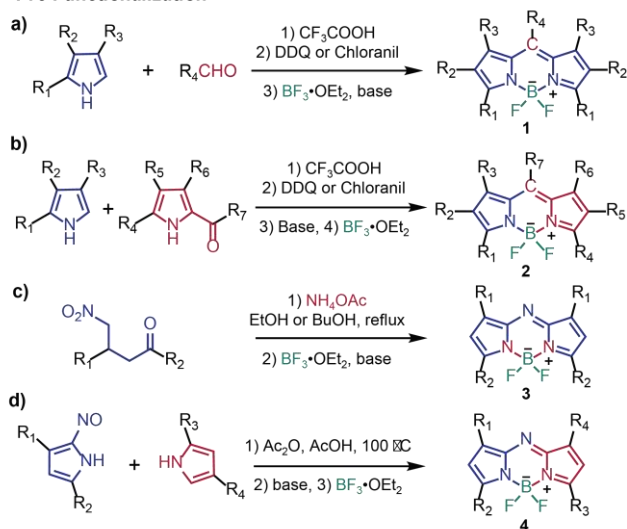


**Scheme 1.** Chemical structures of BODIPY- and azaBODIPY-frameworks, including IUPAC numbering. Note the difference at the “8” *meso*-bridged position from carbon to nitrogen represents the only compositional change resulting in a distinct red-shift in absorption going from BODIPY to azaBODIPY.

## 2.1 Preparation and functionalization of BODIPY

The synthetic pathways toward functionalized BODIPY and its analogue, azaBODIPY, have been the theme of several comprehensive review articles.<sup>23–26</sup> Thus, only general procedures are provided here, and readers are encouraged to refer to the extensive reviews for more detailed information regarding their synthetic preparation. As illustrated in **Scheme 1**, the frameworks of BODIPY and azaBODIPY are nearly identical, yet the subtle change of the atom at the “8” or *meso*-bridged position from the 6<sup>th</sup> element on the periodic table, carbon, to its neighbour nitrogen (the 7<sup>th</sup> element) results in dramatic differences in properties. Most notably is the distinct ~100 nm red-shift in absorption in going from traditional BODIPYs to analogous azaBODIPYs.<sup>8</sup> Since these two unsubstituted frameworks are difficult to access due to the instability of their intermediates, most BODIPYs and azaBODIPYs have at least one substituent on the peripheral pyrrole units. However, the installation of functional groups can dramatically alter several properties, including energy levels that relate to the highest occupied molecular orbital (HOMO) and the lowest unoccupied molecular orbital (LUMO) and thus optical absorption, emission, and redox potentials (described later). The synthesis of substituted BODIPYs and azaBODIPYs can be divided into two general categories: pre-functionalization or post-functionalization, for the installation of substituents before or after the formation of the framework, respectively.

### Pre-Functionalization

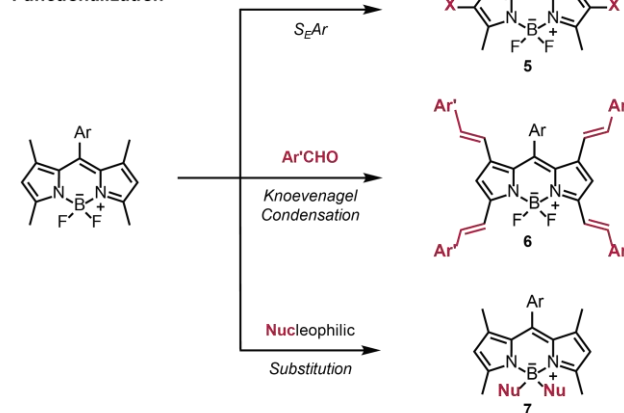


**Scheme 2.** Representative pathways for the pre-functionalization of BODIPY- and azaBODIPY-frameworks, towards symmetric (a)/(c) and asymmetric (b)/(d) derivatives.

Several classic methods for accessing pre-functionalized BODIPY and azaBODIPY frameworks are shown in **Scheme 2**.<sup>2,8</sup> Symmetric BODIPYs (represented by compound **1**) can be synthesized in a stepwise reaction between a substituted pyrrole and aldehyde, with an acid-catalyzed condensation followed by oxidation (**Scheme 2a**). The resulting dipyrromethene intermediate then coordinates with boron trifluoride to afford the final product (**1**). Alternatively, asymmetric BODIPYs (**2**) can be prepared from 2-acylpyrrole and a functionalized pyrrole (**Scheme 2b**). Similar strategies have also been applied to the preparation of pre-functionalized azaBODIPYs **3** and **4** (**Schemes 2c** and **2d**).

An assortment of reactions has been developed for the post-functionalization of BODIPY frameworks (**Scheme 3**).<sup>23</sup> Here, several well-established methods are described using BODIPY for reference, while noting that these approaches also apply to the derivatization of azaBODIPY. Through resonance analysis, it is apparent that the “C2” and “C6” positions on the BODIPY framework carry the greatest partial negative charge, making these positions the most reactive to electrophilic aromatic substitution ( $S_EAr$ ). One of the most common derivatives from this type of reaction is halogenated BODIPY, **5**. As will be disclosed in following sections, these compounds not only have unique photophysical properties, but also can serve as intermediates for further transformations, such as transition-metal catalyzed cross-coupling reactions. Alternatively, the methyl substituents on the “C1”, “C3”, “C5” and “C7” positions are acidic enough to undergo a Knoevenagel condensation with aryl aldehydes.<sup>27,28</sup> The resulting styryl-substituted derivatives, **6**, have extended  $\pi$ -conjugation which results in a bathochromic (red) shift in absorption relative to the precursor. Functionalization of boron can also be accomplished. As revealed by computation, the two electronegative fluorine atoms make boron quite electrophilic.<sup>29</sup> Thus, hard nucleophiles, including alkoxides, Grignards, organolithiums, and acetylides, have been used to directly functionalize the 4-position (boron) to furnish another important class of BODIPY derivatives, **7**.<sup>30–32</sup>

### Post-Functionalization



**Scheme 3.** Representative pathways for post-functionalization of BODIPY frameworks towards three different classes: halogenated, styryl-substituted, and boron-functionalized BODIPYs.

## 2.2 Photophysical and electrochemical properties

### Absorption-Emission, HOMO-LUMO Energies and Redox Potentials

In addition to their facile preparation, BODIPYs are powerful as luminescent dyes, due to their tunable and optimal spectroscopic properties. The BODIPY framework often shows a sharp  $S_1$  (singlet) peak in the visible region ( $>500$  nm) with an extremely large (over  $100,000$   $M^{-1}cm^{-1}$ ) extinction coefficient ( $\epsilon_{max}$ ) that arises from its vertically-allowed Franck-Condon transition.<sup>2,33,34</sup> Moreover, BODIPYs tend to be highly fluorescent with narrow emission bands, where unsubstituted BODIPY providing near quantitative ( $\sim 100\%$ ) emission quantum yield and a moderate excited-state lifetime of  $\sim 6$  ns.<sup>34</sup> Moreover, the properties of BODIPYs can be manipulated by installing various functional groups. In 2014, Peña-Cabrera, Urías-Benavides, and co-workers were able to tailor the wavelength of maximum absorption ( $\lambda_{abs}^{max}$ ) and energy gap ( $E_g$ ) of BODIPY derivatives by attaching different functional groups onto the *meso*-bridged ("C8") position (**Figure 1a**).<sup>35</sup> As supported by density-functional theory (DFT) calculations, the LUMO energy levels were found to be more sensitive to the "C8" substitution relative to the HOMO energy levels, which remained nearly unchanged (**Figure 1b**). This phenomenon was rationalized by the significant depletion of electron density at the "C8" position in the LUMO compared to the HOMO. Therefore, electron-donating groups will typically increase the HOMO-LUMO  $E_g$  by destabilizing (and raising) the LUMO energy level, while electron-withdrawing groups stabilize (and lower) the LUMO, thus decreasing the  $E_g$ .

In 2010, Cosa and co-workers examined the substituent effects at "C2", "C6", and "C8" positions on both the photophysical and electrochemical properties of BODIPYs.<sup>36</sup> Overall, it was shown that the redox potentials, absorption, and emission spectra were all impacted by changes at these positions, demonstrating the versatility and tunability of BODIPY. For example,

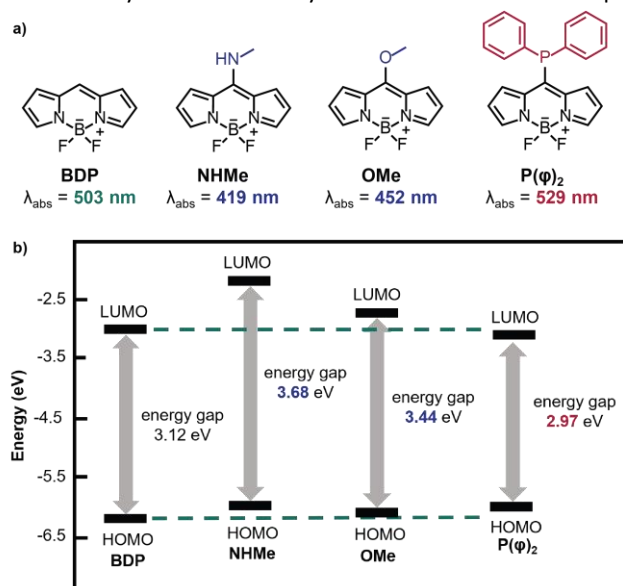


**Figure 1.** The impact of functionalization at the *meso*-bridged ("C8") position on BODIPY absorption and energy levels. a) Chemical structures of various "C8" functionalized BODIPYs and their corresponding wavelength of maximum absorption ( $\lambda_{abs}^{max}$ ); b) Corresponding HOMO/LUMO energy levels determined using DFT. Reproduced from ref. 35 with permission from Wiley-VCH, copyright 2013.

introducing electron-withdrawing groups at the "C2" and "C6" positions led to an increase in both reduction and oxidation potentials, across a wide ( $\sim 0.8$  V) potential range (**Figure 2**). In a subsequent study, the same group further examined inductive effects by performing a Hammett analysis to relate the BODIPY reduction and oxidation potentials to functional groups at the "C2", "C6" and "C8" positions, finding the same trend.<sup>37</sup> While the emphasis of BODIPYs is often placed on their fluorescent behavior ( $S_1 \rightarrow S_0$  transition), certain functional groups have been used to control the ratio of populated singlet-to-triplet excited states (*described later*). However, little-to-no observable room temperature phosphorescence is typically observed for BODIPYs, even though the triplet excited-state yields can be in excess of 60%.<sup>38</sup>

## 2.3 Molecular Photochemistry of BODIPYs

**Electron/Energy Transfer.** Because of its structural rigidity, the non-radiative relaxation of BODIPY's first singlet excited-state is slow, leading to high quantum yields for both photochemical and photophysical reactions. Researchers have leveraged this to utilize BODIPYs in numerous applications, from bioimaging and chemosensors to optoelectronics. Here, common mechanisms applied towards these, and related, end-use applications are described.<sup>33</sup>

**Intramolecular Charge Transfer (ICT).** As disclosed in the previous section, the optoelectronic properties of BODIPY are very sensitive to the electron donating/withdrawing effects of substituents. It has also been demonstrated that the absorption and emission profiles of BODIPYs in dilute solution are greatly impacted by the solvent polarity (solvatochromism). The

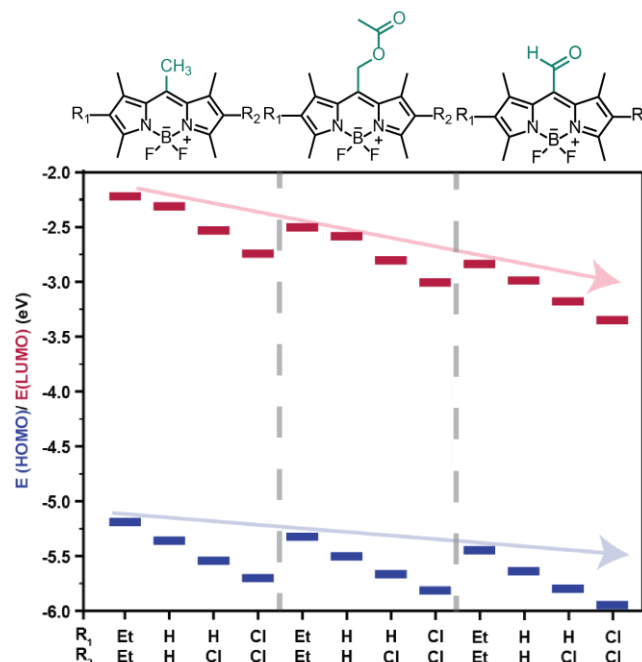
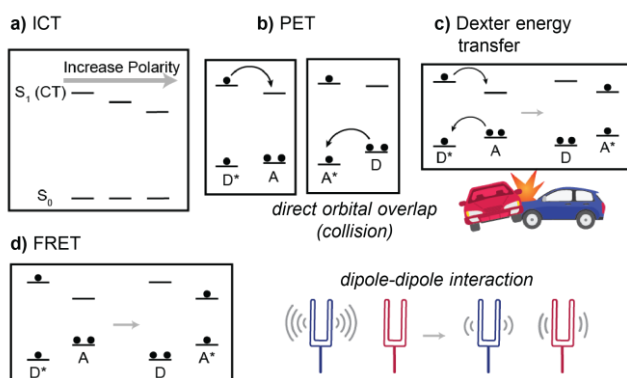


**Figure 2.** The impact of functionalization at the peripheral "C2" and "C6" positions along with the *meso*-bridged ("C8") position on BODIPY energy levels. The general trend is that subtle electronic inductive effects result in significant changes in energy. Here, electron withdrawing groups on the "C2" and "C6" positions are shown to lower both HOMO and LUMO energies. Reproduced from ref. 36 with permission from American Chemical Society, copyright 2010.

solvatochromism is rationalized by the large intramolecular charge-transfer (ICT) character present in the singlet excited-state of many BODIPYs (**Scheme 4a**). Typically, positive solvatochromism is observed, which corresponds to a red-shift of both absorption and emission upon increasing the solvent polarity, which is explained by the stabilization of the ICT state (lowering its energy) and not the ground-state, thus lowering the  $E_g$  (ICT $\rightarrow$ S<sub>0</sub>) (**Scheme 4a**). The sensitivity of BODIPY to polarity-shifts has been used in sensor applications, such as detecting organic solvent vapours, ionic strength, and metal ions, where perturbations in the ICT state results in a visible absorption and/or emission color change.

**Photoinduced electron transfer (PET).** In general, molecules in their photo-excited state are both better reductants (lower ionization potential) and oxidants (higher electron affinity) relative to their corresponding ground-states. PET typically occurs after a photo-excited donor (\*D) and acceptor (A) (or D and \*A) collide (**Scheme 4b**). The rate of electron transfer intuitively rises with increasing temperature, as the number of collisions increase, and plateaus upon reaching a diffusion-limited regime. The highly tuneable HOMO and LUMO energies of BODIPY make it an excellent candidate for light-driven chemical reactions, such as photoredox. Different from the collision-induced PET, molecules where electron donor (D) and acceptor (A) groups are covalently attached [(D)-(Spacer)-(A)] PET occurs directly, with a rate that decreases exponentially as the spacer length increases. In biosensing, covalent attachment has become a common method to achieve emission quenching via PET, which can be altered by separating the D/A through the selective reaction with a target solute (i.e., “turn-on” sensing).

**Dexter Energy Transfer.** Dexter energy transfer is a short distance process ( $\sim$ Å), which can be perceived intuitively as the simultaneous exchange of electrons between the D\* and A (or A\* and D) that results in the D and A\* (or A and D\*) (**Scheme 4c**). As such, Dexter energy transfer is sometimes termed as “Electron Exchange”. Like with PET, its rate and efficiency depend greatly on the orbital overlap (collision), which decreases exponentially with the distance between the D and A.

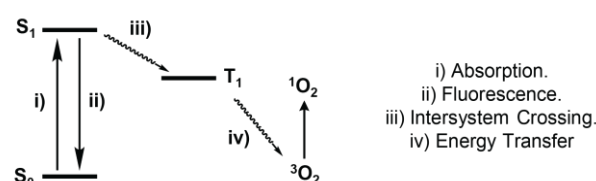


**Scheme 4.** Electron/energy transfer mechanisms. a) Effect of solvent polarity on intramolecular charge transfer (ICT) states; b) Schematic representation of photoinduced electron transfer (PET) and c) Dexter energy transfer that rely on close contact (or “collision”) between a donor (D) and acceptor (A) compound; d) Schematic representation of Förster resonance energy transfer (FRET). D\* or A\*: excited state donor or acceptor, respectively.

**Forster Resonance Energy Transfer (FRET).** FRET is a long distance (1 nm-6 nm) dipole-dipole energy transfer process, originating from the oscillating electric field of D\* then transfer to A. We can visualize the FRET mechanism as a transmitter-antenna and receiver-antenna where the energy transfer operates through space between chromophores and does not require direct orbital overlap (collision) taking place (**Scheme 4d**). The other factor aside from the spatial distance is the “overlapping of states” that is more intuitively viewed as the overlapping of the donor emission spectrum and acceptor absorption spectrum. Combining these two factors, the rate or efficiency of FRET drops inversely to the sixth power of distance ( $\propto 1/R^6$ ) and grows as the absorption/emission spectra overlap more. Using BODIPYs, researchers have applied FRET in biosensing in combination with ICT. For the combined FRET/ICT cases, the chromophores were originally weakly coupled (off-state) and subsequently turned on upon trapping a target analyte resulting in ICT and greater spectral overlap.

**Triplet Formation.** The triplet excited-state population for unsubstituted BODIPY is negligible (<0.1%), as predicted by El-Sayed’s rule: intersystem crossing (ISC) between two electronic states with different multiplicities is forbidden by the conservation of angular momentum. However, one method to overcome this rule and increase the triplet population is by installing atoms of high atomic number (or heavy atoms) to the BODIPY framework, such as halogens (e.g., Cl, Br, and I).<sup>39</sup> These heavy atoms induce strong spin-orbit coupling to facilitate the spin-forbidden transition (e.g. ISC), which has been so aptly named the “heavy atom effect”. One prevalent application of this mechanism among BODIPYs is the generation of reactive singlet oxygen (<sup>1</sup>O<sub>2</sub>), which results from triplet energy transfer (or sensitization) to molecular oxygen that uniquely resides in a triplet ground state (<sup>3</sup>O<sub>2</sub>) (**Scheme 5**). Due to its high reactivity and ease of photochemical generation, singlet oxygen has been applied in many areas, such imaging, photodynamic therapy (PDT), and photocatalysis.<sup>40</sup> In the following discussion, the singlet oxygen generation  $\Phi$  (<sup>1</sup>O<sub>2</sub>) is used as an approximation for triplet quantum yield of functionalized BODIPYs. Here we highlight a few prime and emergent examples of triplet generation in BODIPYs and point the readers toward other review articles focused on the topic for a more in-depth discussion.<sup>4,13,41</sup>

Recently, Costero and co-workers examined the impact of the heavy atom effect on singlet oxygen generation efficiency in halogenated vs non-halogenated BODIPYs by monitoring the decay rate of a known <sup>1</sup>O<sub>2</sub> quencher, DPBF (1,3-diphenylisobenzofuran).<sup>42</sup> The  $\Phi$  (<sup>1</sup>O<sub>2</sub>) for non-halogenated,



**Scheme 5.** Simplified Jablonski diagram for photophysical processes found in various BODIPY systems. S<sub>0</sub>: ground-state. S<sub>1</sub>: First excited singlet state. T<sub>1</sub>: First excited triplet state. <sup>3</sup>O<sub>2</sub>: ground-state oxygen. <sup>1</sup>O<sub>2</sub>: singlet-state oxygen.

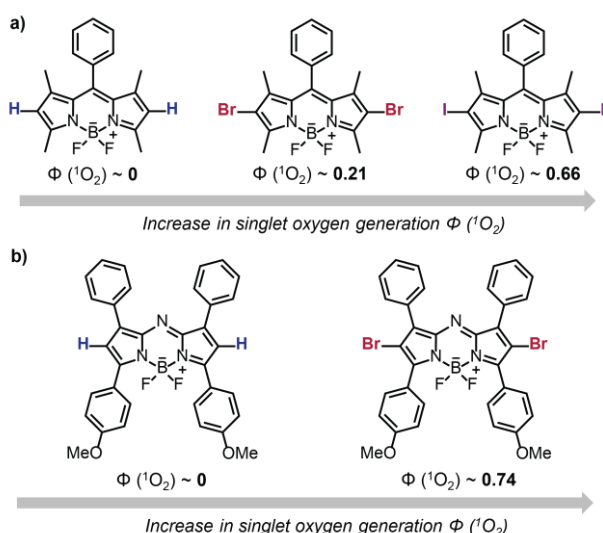
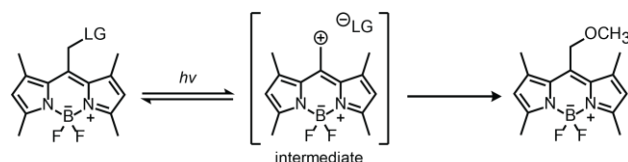


**Figure 3.** Increasing the quantum yield ( $\Phi$ ) of singlet oxygen ( $^1\text{O}_2$ ) generation through halogenation for a) BODIPY and b) azaBODIPY. The high atomic number halogens enhance intersystem crossing rates to increase the triplet yield, which reacts with molecular oxygen ( $^3\text{O}_2$ ) to generate singlet oxygen. Reproduced from ref. 42 and 43 with permission from American Chemical Society, copyright 2004 and 2013.

brominated, and iodinated BODIPYs were found to be approximately 0, 0.2, and 0.6, respectively (**Figure 3a**). This demonstrated the significance of the particular halogen on triplet generation, which was attributed to faster ISC rates in going from -Br to -I, due to stronger spin-orbit coupling. On the other hand, triplet state generation of non-halogenated and brominated azaBODIPY derivatives was investigated by O'Shea and co-workers (**Figure 3b**).<sup>43</sup> The brominated derivative showed a marked improvement in the singlet oxygen generation quantum yield ( $\Phi \approx 0.66$ ) relative to the non-halogenated analogue ( $\Phi \approx 0$ ). Thus, halogenation appears to be a universal strategy to improve triplet yields and in-turn singlet oxygen generation efficiency.

**Photolysis.** Recently, the utility of BODIPYs as photo-protecting groups has received increased attention.<sup>44</sup> In general, photocaged compounds carry "cargo" that is released when "cages" (chromophores) absorb photons of a particular energy or wavelength that cleaves the bond connecting the two together (i.e., photolysis).<sup>45</sup> While *o*-nitrobenzyl photocages are the most commonly utilized systems, they are limited to activation by wavelengths primarily in the ultraviolet region (< 400 nm).<sup>44</sup> Attractively, BODIPY photocages have strong and tunable absorption in the visible region (> 500 nm).<sup>46</sup> For BODIPYs, photolysis results from the mixing of half-filled  $\pi$  and  $\pi^*$  orbitals with filled  $\sigma$  and empty  $\sigma^*$  orbitals upon excitation.<sup>33</sup> In the literature, the relative efficiency of "cargo" release used to compare different photocages is often defined as the maximum extinction coefficient ( $\epsilon_{\text{max}}$ ) multiplied by the chemical quantum yield ( $\Phi$ ), and termed the "uncaging cross-section".

Traditional BODIPY photocages tether the cargo molecules through a carbonate/carbamate linkage on the *meso*-bridged position, which heavily weakens the C-O bond and consequently lowers the  $\sigma^*$  energy to facilitate excited-state



**Scheme 6.** General photocaging mechanism of a *meso* methyl BODIPY containing a leaving group (LG) in a protic solvent (methanol, MeOH), which reacts with the carbocation intermediate.

cleavage. After  $\beta$ -cleavage, a thermal decarboxylation step that emits  $\text{CO}_2$  is required to release the cargo molecule.

Since both carbonate and carbamate linkages can be cleaved by cellular esterases, it might result in undesirable background deprotection. To solve this problem, Weinstein and co-workers demonstrated the first example of direct uncaging of phenols by breaking an ether linkage.<sup>47</sup> Subsequently, Winter, Smith, and co-workers expanded this methodology to the direct release of aliphatic alcohols.<sup>48</sup>

Recently, Klán, Winter, and co-workers systematically designed and synthesized over 30 BODIPY photocage compounds to identify how structure/composition impacts the uncaging efficiency (**Figure 4a**).<sup>49</sup> Ultimately, halogenation of the periphery and alkylation of the boron were found to be the most effective strategies. Specifically, iodination of the BODIPY photocages dramatically enhanced the efficiency more than 40x, which was rationalized by the greatly extended triplet lifetime during which photolysis could occur. Additionally, alkyl-boron BODIPY photocages showed higher uncaging efficiency due to the less electron-withdrawing nature of carbon relative to fluorine, which better stabilizes the positive charge generated at the *meso*-bridged position (**Scheme 6**). Both

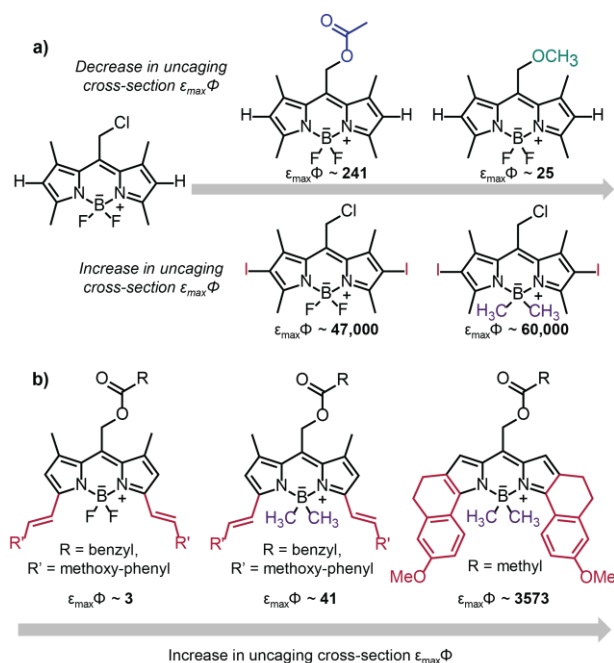


**Figure 4.** Substituent effects on uncaging cross-sections for functionalized BODIPYs. a) Effect of the leaving group (top) and pyrrole iodination and boron methylation (bottom). b) Effect of extended  $\pi$ -conjugation, boron methylation, and ring fusion for BODIPYs with red-shifted absorption. Reproduced from ref. 49 and 50 with permission from American Chemical Society, copyright 2017 and 2018.

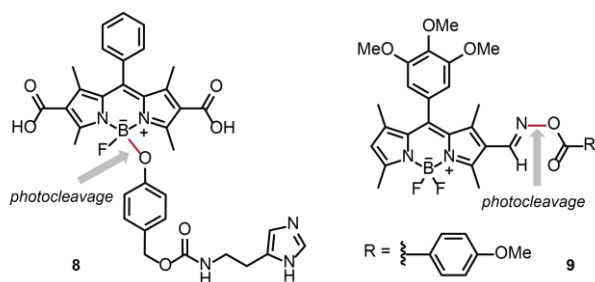


**Figure 5.** Chemical structures for BODIPY photocages with less common photolysis mechanisms occurring at the boron position for compound **8** and the “C2” and “C6” periphery for compound **9**.

strategies were shown to work for a variety of “cargo”, where better leaving groups exhibited higher uncaging efficiencies (e.g., chloride > acetate > methoxide).

In an attempt to leverage the aforementioned effects on derivatives capable of absorbing more benign wavelengths of light, such as far-red (~700-780 nm) and near infrared (> 780 nm), potentially useful in biological applications, Winter, Smith, and co-workers increased the  $\pi$ -conjugation via styryl functionalization. While this shifted the  $\lambda_{abs}^{max}$  from 515 to 661 nm, it unfortunately had a low uncaging cross-section, limiting their applicability (**Figure 4b**).<sup>50</sup> The same group very recently overcame this challenge by conformationally restraining the BODIPY photocages, to inhibit unproductive conical intersections that otherwise decrease the excited state lifetime.<sup>51</sup> Locking the conformation resulted in an impressive ~80-fold increase in uncaging efficiency relative to the styryl counterparts (**Figure 4b**).

Although less common, it is noteworthy to point to the few examples in the literature that have demonstrated photouncaging at positions other than the *meso*-bridged site (**Figure 5**). Specifically, Urano and co-workers synthesized BODIPY-caged histamine **8** where the leaving group was on the boron,<sup>52</sup> and Zhang and co-workers showed a BODIPY photocage, **9**, bearing oxime ester groups capable of photoreleasing carboxylic acids.<sup>53</sup>

### 3. BODIPY-based Polymer Materials

In the third section, we provide an overview on the synthetic incorporation and resultant photophysical properties of BODIPYs covalently attached to a polymer framework. Incorporation into polymers is often accomplished to leverage the distinct advantages they offer over their small molecule counterparts, including improved processability, mechanical flexibility, and biocompatibility. This section is divided into two parts,  $\pi$ -conjugated/cross-conjugated (**section 3.1**) and non- $\pi$ -conjugated (**section 3.2**) BODIPY polymers. Within each part an emphasis is placed on structure-property relationships, including absorption-emission spectra, redox potential, and HOMO-LUMO energy gap, in an attempt to provide a roadmap for readers interested in tailoring such properties for a particular application, with contemporary applications discussed in detail in section 4.

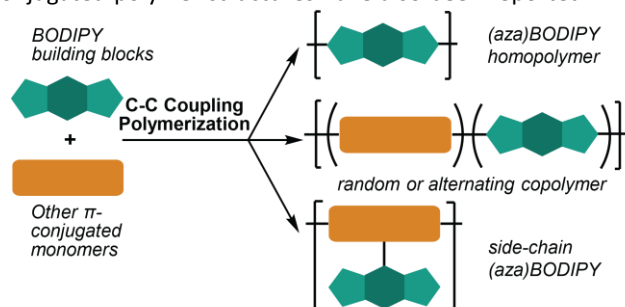
#### 3.1 $\pi$ -conjugated/cross-conjugated BODIPY polymers

Organic  $\pi$ -conjugated polymers combine unique optoelectronic properties with processability to produce lightweight and potentially flexible/stretchable light emitting diodes,<sup>54</sup> field-effect transistors,<sup>55</sup> solar cells,<sup>56</sup> photodetectors,<sup>57</sup> and electrochemical transistors.<sup>58</sup> The tunability of BODIPY's photophysical properties provides a natural intersection with  $\pi$ -conjugated polymers, making it an attractive building block to be incorporated into the electronically coupled framework. To date, this has been accomplished through a number of synthetic methods and provided  $\pi$ -conjugated and cross-conjugated (i.e., partial electron delocalization along the backbone) BODIPY (co)polymers with a range of microstructures (**Scheme 7**).<sup>59</sup>

**Oxidative coupling polymerizations.** Oxidative  $C_{sp2}$ - $C_{sp2}$  bond formation was one of the first methods used to produce  $\pi$ -conjugated polymers and has also found utility with BODIPY building blocks.<sup>60</sup> Oftentimes, this type of polymerization is triggered using chemical oxidants, like  $FeCl_3$ , or by applying anodic potential. While the polymerization mediated by chemical oxidants is generally performed in the bulk as a homogeneous solution to produce solution processable  $\pi$ -conjugated polymers, electropolymerizations are typically performed on surfaces, depositing often insoluble  $\pi$ -conjugated polymer films of controllable thickness on the anode.<sup>61</sup> Potentiodynamic techniques, such as CV, are popular for carrying out electropolymerizations, as they provide mechanistic insight into the redox processes occurring during the early stages of polymerization, and additionally facilitate the examination of the electrochemical behaviour for as-deposited polymer films directly after electrodeposition.<sup>62–64</sup> However, this method is often restricted to polymers with limited solubility, and thus processability, as well as challenges associated with scalability.

#### Transition-metal catalyzed cross-coupling polymerizations.

The more frequently employed synthetic route to BODIPY-based  $\pi$ -conjugated polymers, relies on transition-metal mediated cross coupling reactions, such as Sonogashira, Suzuki, Stille, Kumada, Negishi, and Yamamoto.<sup>65–68</sup> Various polymer microstructures have been accessed through these techniques, including homopolymers,<sup>69</sup> random or alternating copolymers,<sup>70</sup> and side-chain (aza)BODIPY polymers (**Scheme 7**).<sup>71</sup> Furthermore, hyperbranched and microporous BODIPY  $\pi$ -conjugated polymer structures have also been reported.<sup>72</sup> The



**Scheme 7.** General method to synthesize  $\pi$ -conjugated (aza)BODIPY-based polymers and common architectures.

synthetic versatility of BODIPYs has enabled the incorporation at different positions, such as at the periphery, *meso*-bridged, or boron sites, resulting in structural isomers with unique photophysical properties.<sup>73–75</sup>

Analogous to other  $\pi$ -conjugated polymers, planarization and interchain interactions of BODIPY-based polymers can result in significant perturbations to the optoelectronic properties in going from solution to thin films. The resulting difference in optical energy gap can be further amplified through subsequent thermal or solvent annealing processes, which have been leveraged for certain organic electronic applications (discussed later). However, here emphasis is placed on the impact of molecular engineering, or in other words, how changing the composition or structure of BODIPY units in  $\pi$ -conjugated polymers leads to considerable property changes.

**Substituent effects.** As observed with small molecule BODIPYs, changing the composition at the *meso*-bridged position of BODIPYs in  $\pi$ -conjugated polymers can have a dramatic impact on absorption and emission. For example, Chujo and co-workers synthesized twisted phenylene-azaBODIPY alternating copolymers by covalent attachment through aryl substituents on the “C3” and “C5” position (Figure 6a).<sup>76</sup> In comparison to the BODIPY-polymer, **P1**, the azaBODIPY-polymer analogue, **P2**, showed a nearly 100 nm red-shift in peak absorption (in solution), indicating that the inclusion of nitrogen at the *meso*-bridged position results in a substantially reduced HOMO-LUMO energy gap, consistent with that observed for small molecule (aza)BODIPYs. Similarly, altering the *meso*-bridged substituent from methyl (**P3**) to trifluoromethyl (**P4**) in a benzodithiophene-*alt*-BODIPY copolymer resulted in a  $\sim$ 150 nm red-shift in peak absorption (in the solid-state) (Figure 6b).<sup>77</sup> The red-shifted absorption for both the nitrogen and trifluoromethyl functionality is thought to arise from an electron withdrawing inductive effect, which results in a decrease in LUMO energies without significantly perturbing the HOMO energy levels. This hypothesis is supported by computation, where a nodal plane is observed at the *meso*-bridged position for the ground state HOMO, yet a large molecular orbital coefficient appears at the same position in the LUMO state. Therefore, incorporation of an electron withdrawing group at the *meso*-bridged position is thought to be a universal method to decrease the LUMO energy level and in-turn lower the energy gap of BODIPY-based  $\pi$ -conjugated polymers.

The impact of planarization at the *meso*-bridged position can also result in a change in properties. This was demonstrated by Liu and co-workers using phenyl-substituted BODIPY polymers (**P5** and **P6**), where one contained *ortho*-dimethyl substituents, **P5**, twisting the phenyl ring out of plane, and the other contained electron donating methoxy substituents, **P6** (Figure 6c).<sup>78</sup> While only a subtle,  $<10$  nm red-shift was noted (attributed to the electron donating methoxy groups), a significant increase in fluorescence quantum yield was observed for the twisted polymer, **P5** (in solution). This effect was attributed to a restriction in motion of the twisted phenyl ring in **P5** due to steric interactions between the methyl substituents

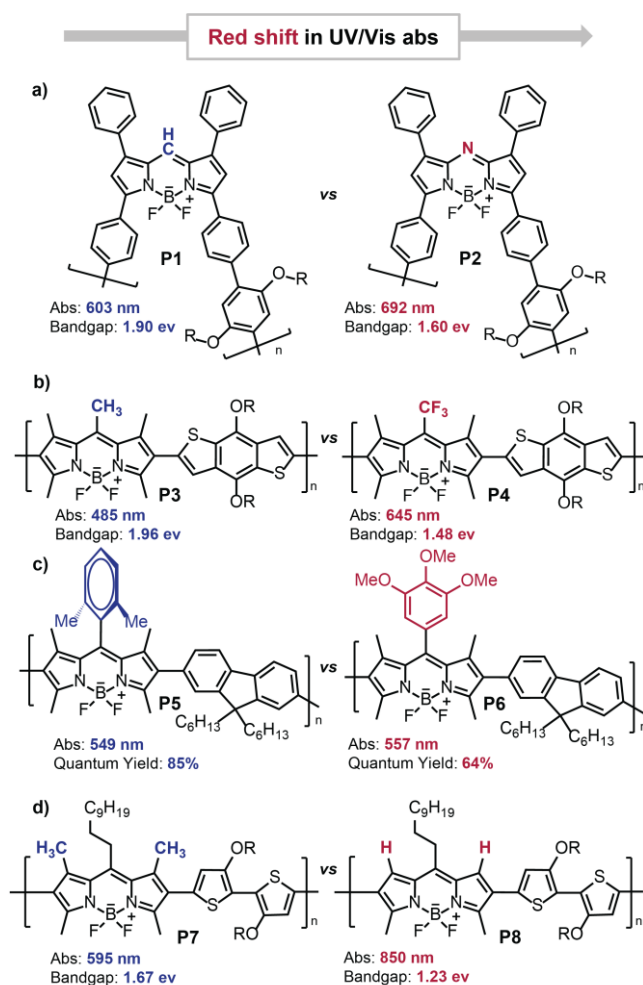


**Figure 6.** Structure-optical relationships of representative  $\pi$ -conjugated BODIPY-based polymers. (a) Chemical structures for poly(phenylene-*alt*-(aza)BODIPY), **P1** and **P2**, showing a red-shifted absorption in solution when replacing the methine bridged group with an aza bridge; (b) Chemical structures for poly(benzodithiophene-*alt*-BODIPY), **P3** and **P4**, showing a red-shifted solid-state absorption in going from a methyl to a trifluoromethyl substituent at the *meso*-bridged position; (c) Chemical structures for poly(flourene-*alt*-BODIPY), **P5** and **P6**, showing an increase in fluorescence quantum yield (in solution) by restricting motion of the phenyl substituent at the *meso*-bridged position; (d) Chemical structures for poly(bithiophene-*alt*-BODIPY), **P7** and **P8**, showing a red-shifted solid-state absorption in replacing the methyl substituents with hydrogen at the “C1” and “C7” positions. Note that absorption (Abs.) reported represents the peak wavelength, while the bandgaps were measured using the low energy band-edge on the absorption spectra. Reproduced from ref 76, 77, and 78 with permission from American Chemical Society, copyright 2009, 2014, and 2018. Reproduced from ref 79 with permission from Wiley-VCH, copyright 2013.

and polymer backbone, which suppresses radiationless decay pathways that are present in **P6** having greater free rotation at the *meso*-bridged position. Therefore, restricting the free rotation of *meso*-bridged groups appended to BODIPY can be employed as a method to enhance photoluminescence quantum yields, potentially useful in lighting or imaging applications.

Besides altering the functionality at the *meso*-bridged position, substituents on other positions of the BODIPY framework have also been shown to impart a significant influence on the polymer properties. Facchetti, Stoddart, Usta, and co-workers synthesized bithiophene-*alt*-BODIPY copolymers **P7** and **P8**, and

discovered a  $\sim 250$  nm red-shift in absorption (in the solid state) by simply altering the substituents at the "C1" and "C7" from methyl (**P7**) to hydrogen (**P8**), as shown in **Figure 6d**.<sup>79</sup> It was hypothesized that the large red-shifted absorption resulted from an increased backbone planarity, resulting in improved  $\pi$ - $\pi$  stacking in thin films.

**Pendent BODIPYs.** To examine the impact of a different  $\pi$ -conjugated polymer architecture on photoluminescence properties Burgess and co-workers prepared a series of cross-conjugated poly(fluorene-co-phenylBODIPY) materials where the BODIPY unit resided as a side-chain in  $\sim 19$ -25 mol% relative to fluorene (**Figure 7a**).<sup>80</sup> The underlying hypothesis was that energy harvested via the strong absorptivity of the major fluorene component would be transferred to BODIPY for longer wavelength emission. Indeed, after excitation at 358 nm, these BODIPY-incorporated polyfluorenes emitted brightly at 517 nm (**P9**) and 677 nm (**P10**), where the  $\sim 160$  nm emission red-shift resulted from enhanced planarity and partial electron delocalization into the pendent BODIPY on **P10**. The demonstrated utility in bioimaging was accomplished with these polymers by fabricating polymer nanoparticles from them and embedding them into cells, as shown in **Figure 7b**. Another method that has been employed to incorporate cross-conjugated BODIPY side-chains and tailor optoelectronic properties of the polymer main-chain is through post-polymerization modification, such as through a Knoevenagel condensation reaction on "C1", "C3", "C5", and "C7" methyl substituents or boron-oxygen complexation.<sup>81</sup>

**Planarization and Donor-Acceptor Effects.** As red-shifting absorption/emission is desirable for a number of applications in both imaging and organic electronics, unique methods to this end have been developed, beyond what has been described previously. For example, incorporating an acetylene or vinylene

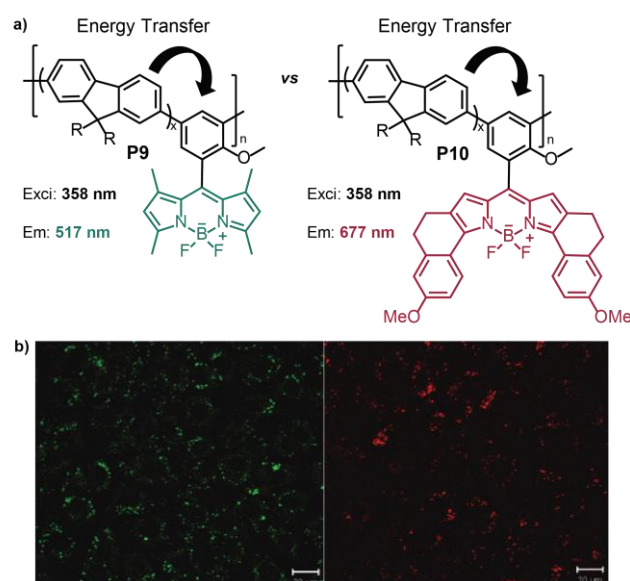


**Figure 7.** Side-chain BODIPY  $\pi$ -conjugated polymers with energy transfer for fluorescence imaging. a) Structures of polyfluorenes with different BODIPY pendent groups having green (**P9**) and red (**P10**) emission; b) Confocal image of Clone 9 rat liver cells with **P9** (left) and **P10** (right). Data and images were adopted with permission from reference 80. Copyright (2011) American Chemical Society.

bridge between BODIPY results in a pronounced bathochromic shift ( $>150$  nm) in absorption/emission, which is attributed to planarization, and thus extension of the maximum  $\pi$ -conjugation length to reduce the bandgap.<sup>70</sup>

The bandgap can also be reduced by combining electron rich donor (D) repeat units with electron deficient acceptor (A) units.<sup>82,83</sup> For D-A conjugated polymers the HOMO is primarily located on the donor unit, while the LUMO resides primarily on the acceptor unit. In addition to stabilization of the lower energy gap quinoid-like form that occurs along the polymer backbone in D-A structures, energy level hybridization between the donor and acceptor also reduces the bandgap (**Figure 8a**). Drawn by these merits, numerous  $\pi$ -conjugated D-A polymers

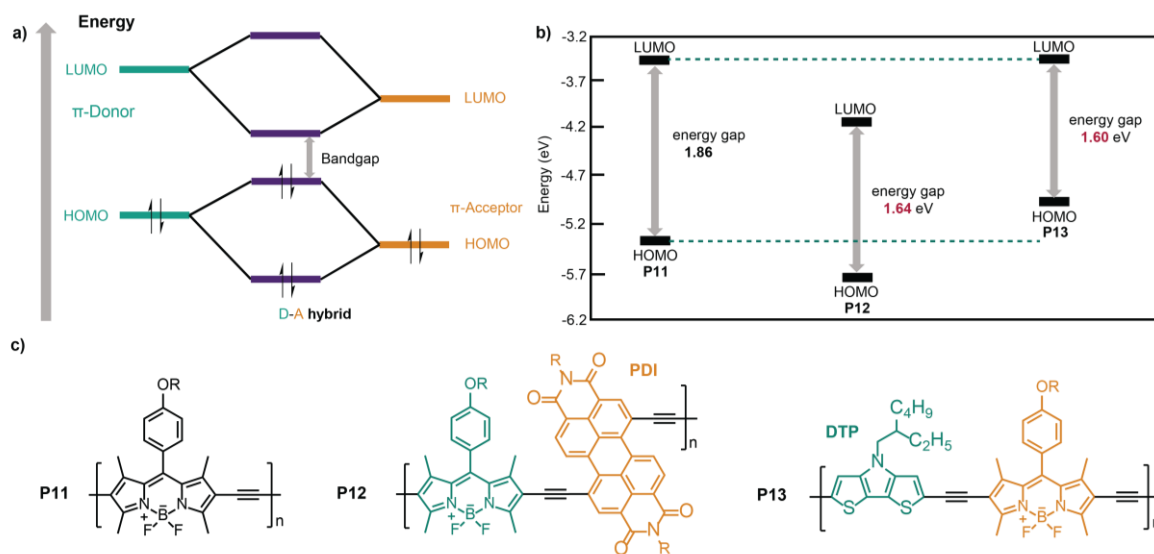


**Figure 8.** Donor-acceptor (D-A)  $\pi$ -conjugated BODIPY polymers produced by Sonogashira coupling. a) D-A orbital hybridization to narrow the bandgap. b) Energy level diagram for **P11**, **P12** and **P13**. c) Chemical structures for polymers **P11**, **P12**, and **P13**. Incorporation of PDI as an acceptor resulted in lowering both the HOMO and LUMO energy levels, while incorporating DTP as a donor raised the HOMO energy level. HOMO: highest occupied molecular orbital; LUMO: lowest occupied molecular orbital; D = donor (green); A = acceptor (orange); PDI = perylene diimide; DTP = dithienopyrrole. Reproduced from ref. 84 with permission from American Chemical Society, copyright 2011. Reproduced from ref. 85 with permission from the Royal Society of Chemistry, copyright 2012.

incorporating (aza)BODIPY units have been published. Given the versatility of (aza)BODIPYs examples exist where the BODIPY serves as either the donor or acceptor group in the conjugated polymer. For example, Thayumanayan and co-workers performed a systematic examination on a series of alternating acetylenic BODIPY copolymers, synthesized via Sonogashira polycondensation, where the composition of the BODIPY repeat unit was held constant (**Figure 8c**).<sup>84,85</sup> In comparison to the BODIPY homopolymer control, **P11**, incorporation of perylene diimide, PDI, as a  $\pi$ -acceptor (**P12**) stabilized (and thus lowered the energy of) both HOMO and LUMO energy levels, reducing the energy gap from 1.86 eV (**P11**) to 1.64 eV (**P12**) (**Figure 8b**). In contrast, copolymers comprising the same BODIPY repeat unit with dithienopyrrole (DTP) as an electron rich donor (**P13**) resulted in an increase in the HOMO energy level and little change in the LUMO energy level, resulting in a net decrease of the energy gap to 1.60 eV. (**Figure 8b**). Results from CV analysis confirmed that **P13** (with DTP) possessed the highest HOMO energy. It was noted that the LUMO energy levels of these BODIPY polymers remain invariant regardless of the choice of comonomer, suggesting that the BODIPY moiety had a primary influence on LUMO levels of the polymer (**Figure 8b**).

A number of other D-A  $\pi$ -conjugated BODIPY polymers exist in the literature, as well as azaBODIPYs, with a notable extreme set of polymers prepared by Chochos and co-workers using Stille polycondensation. In this example an ultra-low optical energy gap of  $\sim 0.85$  eV ( $\sim 1.25$  eV electrochemical energy gap) with poly(quarterthiophene-*alt*-thienylBODIPY), **P14**, was achieved (**Figure 9**).<sup>86</sup> In addition to incorporating a strong electron rich quarterthiophene donor repeat unit, the bandgap was further reduced by incorporating a thienyl substituent at the *meso*-bridged position on the BODIPY repeat unit leading to  $\pi$ -extension, and by removing the substituents often present on the pyrrole periphery to enhance planarization. The charge transporting characteristics of these polymers were also examined in thin film transistors, demonstrating their utility with modest hole mobility values ( $\mu_h \approx 10^{-4}$  cm<sup>2</sup> V<sup>-1</sup> s<sup>-1</sup>).

**Chiroptical BODIPYs.** Although  $\pi$ -conjugated polymers have largely been exploited for their unique fluorescence (imaging) and charge transporting (organic electronics) properties,

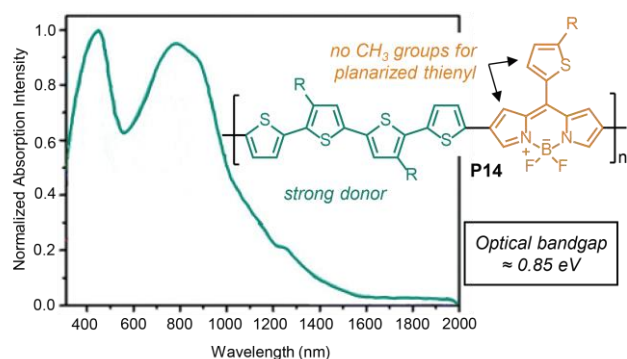


**Figure 9.** Absorption spectrum and chemical structure for an ultra-low bandgap poly(quarterthiophene-*alt*-thienylBODIPY). The combination of a strong donor-acceptor pair and planarization/extended conjugation from the lack of pyrrole substituents contributes to the reduction in bandgap. Reproduced from ref. 86 with permission from the Royal Society of Chemistry, copyright 2018.

another unique and exciting property recently demonstrated with BODIPY-based  $\pi$ -conjugated polymers is polarized emission, with potential utility in photoelectric devices.<sup>87</sup> Introducing  $\pi$ -conjugated chiral repeat units has been used to afford chiroptical properties, specifically circularly polarized luminescence. For example, Cheng, Li, and co-workers reported a series of chiral binaphthyl-BODIPY  $\pi$ -conjugated polymers via Sonogashira cross-coupling and showed efficient circularly polarized luminescence (CPL) of red light with high fluorescence quantum yields of  $\sim 25\%$  (**Figure 10**).<sup>88</sup>

### 3.2 Non- $\pi$ -conjugated BODIPY polymers

**Synthesis.** In contrast to conjugated polymers where BODIPY is typically located in the main-chain, non- $\pi$ -conjugated polymers often append BODIPYs as side-chains through two general methods, “grafting-through” (**Scheme 8a**) and “grafting-to” (**Scheme 8b**). The first method, grafting-through, is where BODIPYs are functionalized with polymerizable moieties (e.g., (meth)acrylate,<sup>89</sup> (meth)acrylamide,<sup>90</sup> and styrene<sup>91</sup>), typically off the *meso*-bridged position, and incorporated directly into the main-chain via polymerization. Although most of the grafting-through pathways are based on radical chain-growth mechanisms, there are a few references relying on olefin metathesis polymerizations (e.g., acyclic diene metathesis<sup>92</sup> and ring opening metathesis polymerizations<sup>93</sup>). The other method is “grafting-to”, which is a post-polymerization modification approach. Besides traditional coupling reactions, “click chemistries”, including Cu<sup>I</sup>-catalyzed azide/alkyne cycloaddition (CuAAC),<sup>94</sup> thiol-ene,<sup>95</sup> thiol-Michael,<sup>96</sup> and Diels-Alder reactions,<sup>97</sup> have been used to functionalize polymers with BODIPYs. In addition to side chain functionalization, BODIPYs can also be positioned at chain ends or the middle of a chain via direct polymerization from BODIPYs functionalized with initiators.<sup>98</sup> As the incorporation of BODIPYs in non- $\pi$ -conjugated polymers does not result in extension of the  $\pi$ -

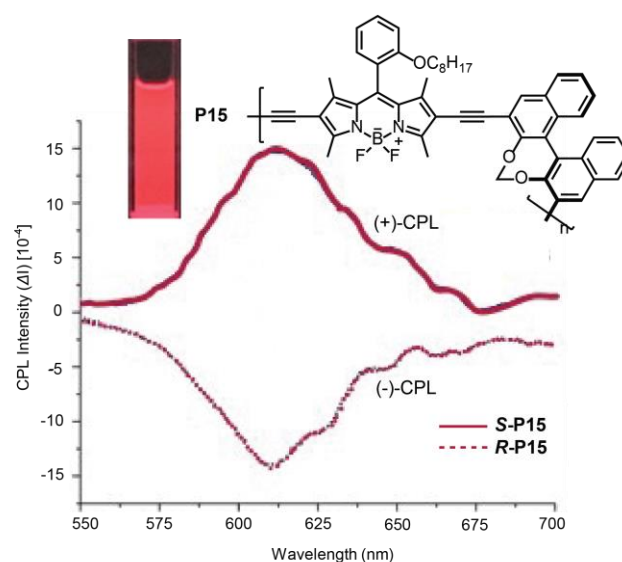
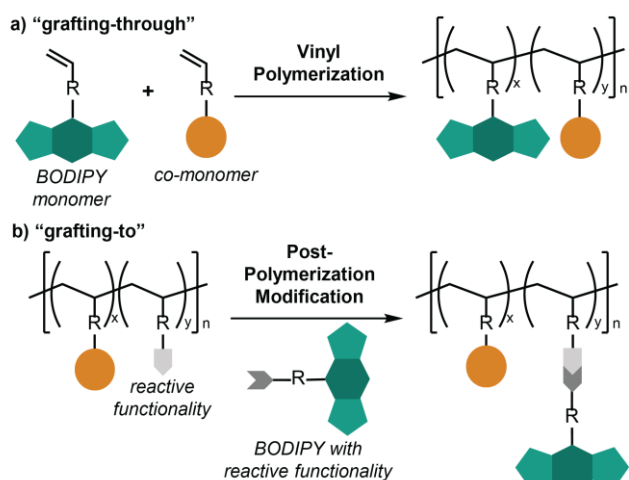


**Figure 10.** Chiral photoluminescence (CPL) of helical  $\pi$ -conjugated BODIPY. The incorporation of R/S-methylenedioxy-binaphthyl results in the formation of a helix that outputs circularly polarized light. Inset shows photoluminescence from **P15**. Circular dichroism spectrum adapted from reference 88. Copy right (2016) American Chemical Society.



**Scheme 8.** Synthetic pathways to access non-conjugated polymers incorporating (aza)BODIPYs

system, certain optical properties are indistinguishable between monomeric BODIPYs and their corresponding polymers. However, photoluminescent properties of non- $\pi$ -conjugated BODIPY polymers have been manipulated by tailoring the polymer microstructure.

**Polymer particles.** Tailoring the spatial location of BODIPYs in non- $\pi$ -conjugated polymer particles has been used as a method to control photoluminescent properties. For example, Clavier and co-workers carried out a systematic investigation using two BODIPY monomers functionalized with styrene and methacrylate (**Figure 11a**).<sup>99</sup> Following a one-pot miniemulsion reversible addition fragmentation chain transfer (RAFT) polymerization, fluorescent core-shell nanoparticles were formed (**Figure 11b**). The microstructures of the resultant copolymers were governed by the nature of the polymerizable handle (e.g., styrenic or methacrylic) on the BODIPYs, which corresponded to their reactivity ratios with styrene. It was found that polymer particles synthesized with BODIPY monomers bearing a styrenic handle (**P16**) showed increased brightness (by a factor 2) relative to those produced with acrylate-functionalized BODIPYs (**P17**). These results highlighted the importance of BODIPYs' spatial location in the fluorescent core-shell nanoparticles on the overall photoluminescent properties. Subsequent reports from the same group examined other factors, including the effect of BODIPY concentration in the copolymers and the architecture of the hydrophilic blocks. It was found that increasing the BODIPY concentration lowers both the overall fluorescence quantum yield and lifetime, yet brightness of individual particles were higher.<sup>100</sup> Alternatively, switching the architecture of hydrophilic blocks from linear to comb-like results in particles with a void in the center (i.e. nanocapsules) that exhibit higher fluorescence quantum yield, brightness, and fluorescence lifetime compared to their core-shell nanoparticle counterparts.<sup>101</sup> These structure-property relationships are important to consider when designing novel BODIPY- (or other dye-) functionalized polymer particles with potential applications in sensing and imaging.

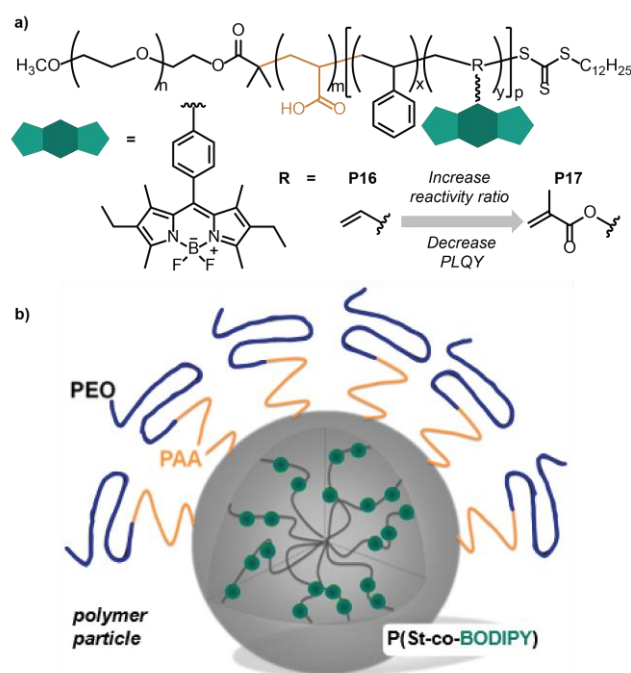


**Figure 11.** Non- $\pi$ -conjugated BODIPY polymer particles. a) Chemical structure of block copolymers **P16** and **P17**; PLQY: photoluminescence quantum yield. b) Schematic representation of the fluorescent core-shell nanoparticles. Altering the spatial incorporation of BODIPY units within the core-shell from **P16** (random incorporation) to **P17** (non-random incorporation) directly impacts photoluminescence, with **P16** providing brighter particles than non-random incorporation with **P17**. Figure adapted with permission from reference 99. Copy right (2013) American Chemical Society.

**Stimuli responsive behavior.** The photoluminescent properties of non- $\pi$ -conjugated BODIPY functionalized polymers can also be controlled using non-contact external stimuli, such as heat and light, which is attractive for potential biomedical applications where on-demand triggering, such as for drug-release, is desirable and having a corresponding signal, such as photoluminescence, to indicate successful stimulus activation would be beneficial. For example, Liras and co-workers prepared thermoresponsive polymethacrylates **P18** containing a small fraction of BODIPY functionalized repeat units ( $\sim 0.7$  mol%) (**Figure 12a**).<sup>102</sup> The polymers exhibited a lower critical solution temperature (LCST) at  $\sim 35$  °C, below which the polymers were solvated, forming extended chains in solution with minimal fluorescence. Heating above the LCST leads to rapid chain collapse and a simultaneous increase in emission quantum yield by a factor of  $\sim 1.5$ , which is attributed to suppressed rotation of BODIPY units. Furthermore, this process was shown to be reversible with no loss in emission after six cycles. Subsequently, the same polymer was incorporated into thermoresponsive hydrogels demonstrating once again a reversible photoluminescence change upon crossing the LCST.<sup>102</sup>

As a complement to thermal triggering, Jiang, Yi, Chen, and co-workers prepared photo-switchable fluorescent non- $\pi$ -conjugated polymers **P19** (**Figure 12b**).<sup>89</sup> Specifically, they developed fluorescent nanoparticles containing a hydrophobic block comprising methyl methacrylate, BODIPY methacrylate, and spiropyran methacrylate repeat units. Upon irradiation with UV light ( $\sim 302$  nm), a stark drop in fluorescence intensity

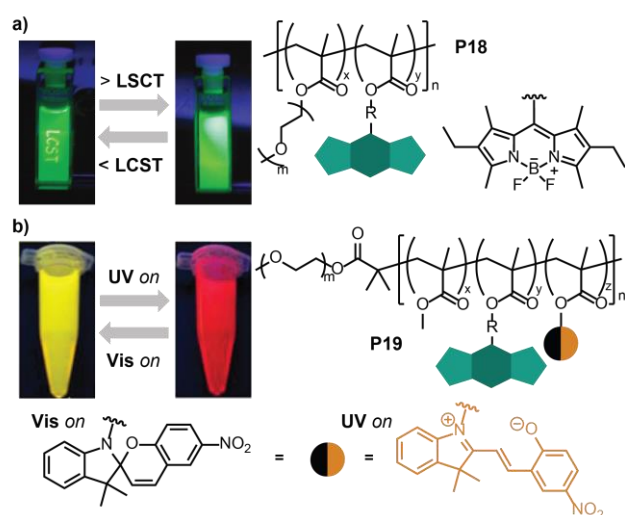


**Figure 12.** Switching behavior of photoluminescence. a) heat-induced switching of **P18**. LCST: lower critical solution temperature. Figure adapted with permission from reference 102. Copy right (2011) American Chemical Society. b) light induced switching of **P19**. UV: light irradiation at 305 nm. Vis: light irradiation at 525 nm. Figure adapted with permission from reference 89. Copy right (2015) American Chemical Society.

at 550 nm was observed. However, upon irradiating with visible light ( $\sim 525$  nm) for 10 mins, the fluorescence intensity nearly fully recovered. This phenomenon was attributed to intraparticle FRET between the BODIPY units and the merocyanine states of neighboring spiropyran units. The utility of light as a stimulus as opposed to heat offers attractive benefits including the potential to be more benign (for low energy visible light) especially in a biological setting where small fluctuations in temperature or pH can be toxic, along with offering precise control over where and when triggering occurs (i.e., spatiotemporal control).

## 4. Applications of BODIPY in Polymer Science

The tunability of the BODIPY platform is exemplified by its versatility in applications, ranging from medicine to optoelectronics and light driven catalysis. Here, the cutting-edge applications that have resulted from integrating BODIPYs with polymers are summarized. First, the utility of BODIPYs as “fluorescent probes” to examine fundamental polymer properties is described (section 4.1). Subsequently, the applications of BODIPYs in both  $\pi$ -conjugated and non- $\pi$ -conjugated polymers are emphasized, including imaging, photodynamic therapy, solar cells, thin-film transistors, chemosensors, and heterogeneous photocatalysts for organic synthesis (section 4.2). We conclude by emphasizing the nascent utility of BODIPYs in the preparation and degradation of synthetic polymers (section 4.3).

### 4.1 BODIPYs to examine fundamental polymer properties

Both fluorescence spectroscopy and microscopy are non-invasive techniques that have proven invaluable in characterizing and visualizing both synthetic and living systems, facilitating research into the structure and dynamics of (bio)polymers in ensembles and at the single molecule level.

Due to their remarkable photophysical properties, BODIPYs have served as indispensable fluorophores in these endeavours.

**Molecular weight characterization.** Polymers labelled with BODIPY fluorophores have been utilized in fluorescence correlation spectroscopy to determine the hydrodynamic radius and thus estimate of molecular weight. However, initial models were created for monodisperse (single molecular weight) polymers, making the assessment of inherently disperse synthetic polymer samples particularly challenging. Furthermore, Koynov and co-workers synthesized polystyrene and poly(methyl methacrylate) via controlled radical polymerization, and found that it was critical to label the polymer chains with only one BODIPY chromophore to provide accurate number-average values of hydrodynamic radius for the disperse (molecular weight) samples.<sup>98</sup> To preclude the need to functionalize polymer chains with only one chromophore, the authors developed a new model based on the Schulz-Zimm distribution function for fitting autocorrelation curves from fluorescence correlation spectroscopy, making the technique more broadly applicable.

**Morphological characterization.** As a complement to more traditional electron diffraction methods, fluorescence microscopy has been employed to directly visualize BODIPY-labelled synthetic polymers to assess self-assembled morphologies. An elegant example of this was reported by Manners and co-workers, synthesizing a series of polyferrocenyldimethylsilane-*block*-(poly(dimethylsioxane)-*random*-poly(methylvinylsiloxane)) (PFS-*b*-(PDMS-*r*-PMVS)), in which the PMVS segments were functionalized with one of three different BODIPY units having distinct blue (**P20**), green (**P21**), or red (**P22**) emission (Figure 13a).<sup>103</sup> Leveraging the crystallisable PFS block, crystallization-driven self-assembly (CDSA) revealed block co-micelles with well-defined segments (Figure 13b). Due to the presence of different BODIPY-modified block copolymers, fluorescence microscopy was used to confirm the spatially defined nanosegregation of each domain by simply noting the distinct emission colours (Figure 13c). Up to 11-block co-micelles were demonstrated with CDSA via sequential addition of the three fluorescent block copolymers, showing stability over a period of months with no detectable diffusion or mixing of the luminescent polymers. Subsequently, the same group has applied this strategy to also fabricate fluorescent concentric rectangular platelet block comicelles as a different morphology with multiple and variable fluorescence facilitating the visualization of selected segments.<sup>104</sup>

### 4.2 Applications of polymeric BODIPYs

**Biomedical imaging.** The development of chromophores with high quantum yield far-red to near infrared (700-900 nm) emission has been driven by the utility in *in vivo* fluorescence

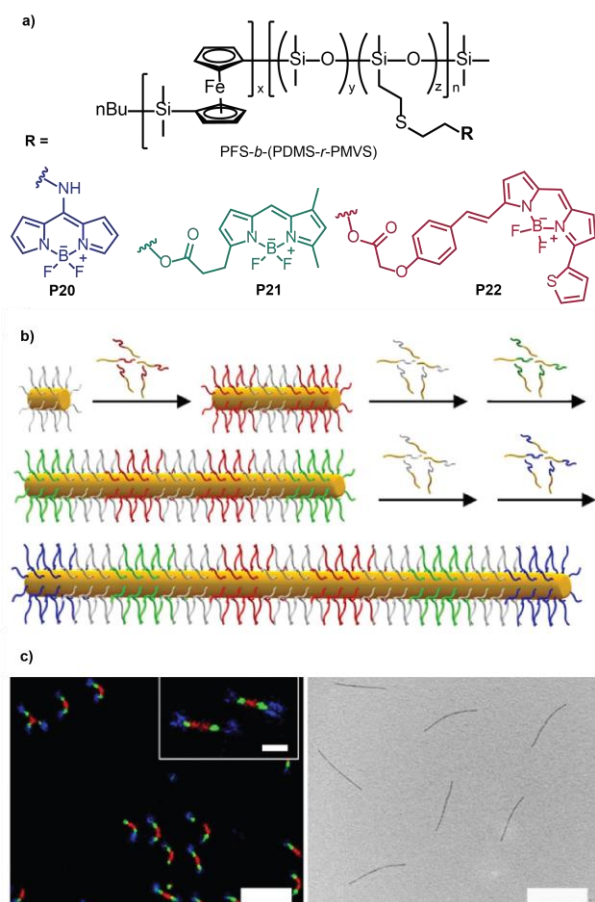


**Figure 13.** Visualization of BODIPY functionalized block co-micelles prepared through crystallization-driven self-assembly (CDSA). a) Chemical structures of polyferrocenyldimethylsilane-*block*-(poly(dimethylsioxane)-*random*-poly(methylvinylsiloxane)) (PFS-*b*-(PDMS-*r*-PMVS)), tagged with distinct BODIPY fluorophores; b) Schematic representation of fluorescent block co-micelles. PFS = yellow, PDMS = grey, fluorescent coronas of **P20**, **P21**, and **P22** = blue, green, and red, respectively; c) Images for self-assembled BODIPY-functionalized block co-micelles under a fluorescence microscope (left) and TEM (right). Scale bars represent 5 and 3  $\mu\text{m}$  for the left and right images, respectively. Images reprinted with permission from reference 103. Copy right (2014) Springer Nature.

imaging. Emission in this long wavelength region provides access to an “optical window” in living systems, as both background interference and in-tissue photon absorption/scattering are low relative to shorter wavelength visible and UV light. Naturally, the excellent processability and biocompatibility of synthetic (aza)BODIPY polymers combined with their bright emission of far-red (700-780 nm) or even NIR (> 780 nm) light has led to their utility as powerful fluorescence probes for *in vivo* biomedical imaging.

Chiu, Wu, and co-workers pioneered the development of long-wavelength-excitabile  $\pi$ -conjugated polymer dots (LWE-Pdots), which provided bright emission of visible light through an energy transfer mechanism between a donor and acceptor chromophore.<sup>105</sup> In 2019, expanding upon this work, the same authors prepared BODIPY-functionalized polymers **P23** and **P24**, which underwent nanoprecipitation with **P25** to afford two types of Pdots (**Figure 14a**).<sup>106</sup> The ternary Pdots (**P23+P24+P25**) had bright far-red emission that resulted from a combination of high absorption coefficients and fluorescence quantum yields ( $\approx 40\%$ ). In comparison to binary Pdots (**P24+P25**) and commercially available quantum dots (Qdot-705), the brightness was nearly 5-fold and 14-fold larger, respectively, representing a significant advancement in imaging. The photoluminescence mechanism in the ternary Pdot system starts with excitation of the BODIPY in **P23** ( $\lambda_{abs}^{max} = 532\text{ nm}$ ), followed by energy transfer to the BODIPY in **P24** that then emitted far-red light ( $\lambda_{PL}^{max} = 721\text{ nm}$ ). Additionally, the brightness was enhanced by suppressing the self-quenching pathway that occurs upon BODIPY H-aggregate formation by dilution with poly[(9,9-dioctyl-fluorene)-*alt*-(4,7-di-2-hexylthienyl-2,1,3-benzothiadiazole)] (PFDHTPT) repeat units in the copolymer. The application of these Pdots in *in vivo* bioimaging was examined for tumor-bearing nude mice, showing improved whole-body fluorescence relative to both binary Pdots and commercial Qdot-705 (**Figure 14b**).

As an alternative approach Cheng, Zhang, Xu, and co-workers showed that non- $\pi$ -conjugated polymer nanoparticles (NPs) bearing an azaBODIPY with far-red emission were effective

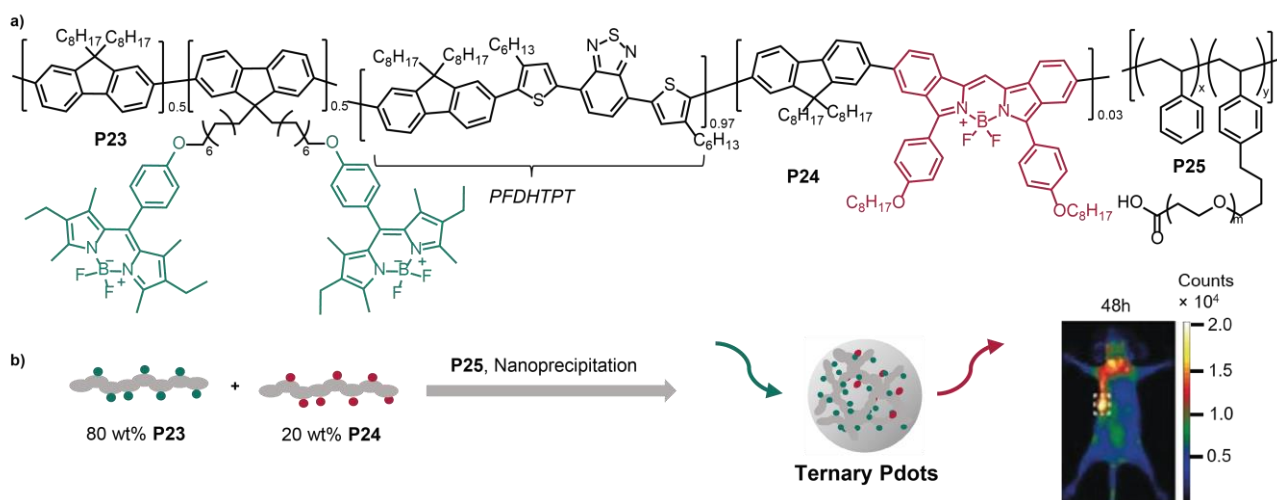


**Figure 14.** Long-wavelength-excitabile  $\pi$ -conjugated polymer dots (Pdots) bearing BODIPYs for bioimaging. a) Chemical structures of functional (aza)BODIPY copolymers, **P23** and **P24**, and polymer used to facilitate nanoprecipitation, **P25**; b) Schematic representation of the nanoprecipitation process used to create binary and ternary Pdots, along with a respective fluorescence image from *in vivo* experiments. Images reprinted with permission from reference 106. Copy right (2019) Wiley-VCH.

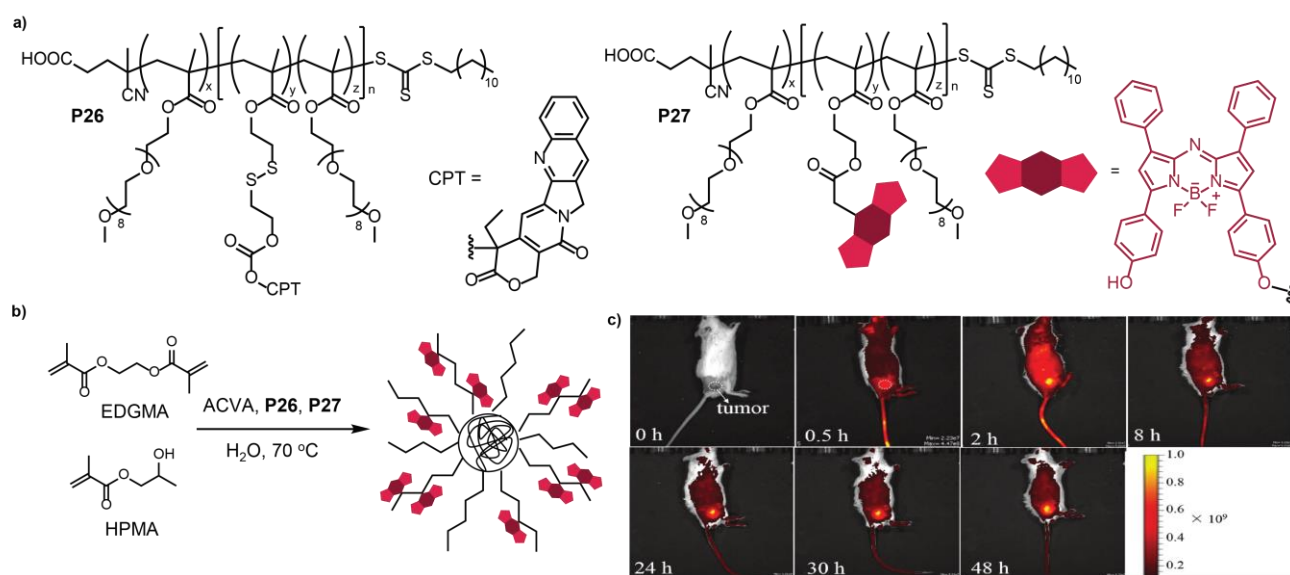


**Figure 15.** Non- $\pi$ -conjugated polymer nanoparticles (NPs) bearing an anticancer drug, camptothecin (CPT), **P26**, and an azaBODIPY chromophore, **P27**. a) Chemical structures of macro-RAFT (chain-transfer) agents; b) Schematic representation of the NP fabrication process using reversible addition fragmentation chain-transfer (RAFT) polymerization with ethylene glycol dimethacrylate (EDGMA) and 2-hydroxypropyl methacrylate (HPMA) to form the NP corona; c) Fluorescence images from *in vivo* experiments monitoring the location of the polymer pro-drug. Reproduced from ref. 107 with permission from the Royal Society of Chemistry, copyright 2018.

bioimaging agents.<sup>107</sup> In this report, two macro-RAFT agents **P26** and **P27** (Figure 15a) bearing the anticancer drug camptothecin (CPT) and azaBODIPY, respectively, were synthesized and incorporated into polymeric NPs through crosslinking with ethylene glycol dimethacrylate (EDGMA) and 2-hydroxypropyl methacrylate (HPMA) via RAFT (Figure 15b). In this grafting-from approach, both the anticancer drug and azaBODIPY chromophore were envisioned to reside on the periphery of NPs to enhance both drug availability and emission from reduced aggregation, as depicted in Figure 15b. These dual-functional NPs, with narrow size and controlled drug-loading capacity, were shown to kill cervical cancer (HeLa) cells, where spatial monitoring in real-time was possible due to *in vivo* fluorescence imaging (Figure 15c).

**Photodynamic therapy.** As mentioned previously, BODIPYs with high singlet oxygen ( $^1\text{O}_2$ ) quantum yield ( $\Phi$ ) and absorption in the far-red region are excellent candidates for photodynamic therapy (PDT).<sup>4</sup> In addition to efficient generation of reactive  $^1\text{O}_2$  that can kill cancer cells, BODIPYs can simultaneously facilitate *in vivo* visualization via fluorescence emission.<sup>108</sup> Han and co-workers demonstrated this by encapsulating a carbazole-substituted BODIPY with an amphiphilic diblock copolymer, polylactide-*block*-polyethylene glycol (PLA-*b*-PEG) (**P28**) chain-end functionalized with a tumor targeting agent, folate (Figure 16a).<sup>109</sup> The BODIPY was selected for its strong and broad absorption band in the far-red to NIR region (~600–800 nm), and a high  $\Phi$  ( $^1\text{O}_2$ ) of ~67%. Encapsulation of the BODIPYs into **P28** provided uniform NPs that were water soluble and demonstrated tumor targeting capabilities, as observed with fluorescence imaging (Figure 16b). The BODIPY fluorescence was used to noninvasively guide PDT and monitor the results, finding that an exceptionally low-power-density halogen lamp (12 mW/cm<sup>2</sup>, 670–800 nm) provided an unprecedented deep-tissue photodynamic therapeutic effect.

In this application, it was also shown that the polymer was required to effectively stabilize the BODIPY under *in vivo* conditions, signifying the importance of the polymer-BODIPY combination.

**Organic electronic devices.** Given the  $\pi$ -conjugation intrinsic to BODIPYs and the numerous examples of incorporating BODIPYs

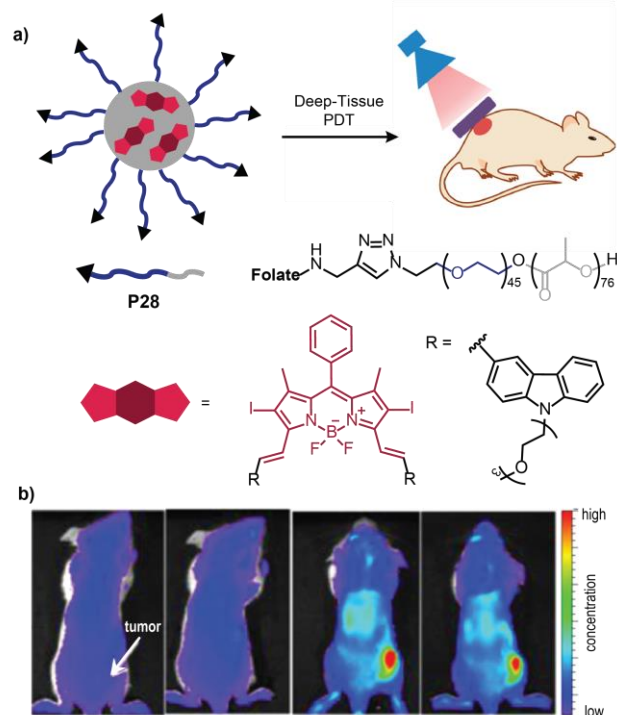


**Figure 16.** Photodynamic therapy (PDT) using a far-red absorbing and singlet oxygen generating halogenated BODIPY encapsulated within a polymer particle. a) Schematic illustration of deep-tissue PDT and chemical structures for the polymer particle components. b) Time dependent *in-vivo* fluorescence imaging showing localization of the polymer particles by the tumor. Figure adapted with permission from reference 109. Copy right (2016) American Chemical Society.

into  $\pi$ -conjugated polymers, they have found natural utility in organic electronic devices.<sup>9</sup> This sub-section is divided into two parts, featuring applications in solar cell and organic thin-film transistor (OTFT) devices. Thanks to breakthroughs in the design and fabrication of organic semiconductors, solar cells have emerged as a feasible source of low-cost renewable energy, while OTFTs offer a flexible and lightweight alternative technology to conventional transistors found in every-day microelectronics (e.g., cell phones and computers).

**Solar Cells.** In 2010, Fréchet and co-workers pioneered the examination of BODIPY functionalized polymers in bulk heterojunction (BHJ) solar cells.<sup>110</sup> In these first devices, an acetylenic  $\pi$ -conjugated BODIPY-*alt*-thiophene polymer, **P29**, was blended with [6,6]-phenyl-C<sub>61</sub>-butyric acid methyl ester (PC<sub>61</sub>BM), providing a sunlight-to-electricity efficiency, or power conversion efficiency (PCE), of 2% (Figure 17). In these bulk heterojunction solar cells **P29** acted as the primary light absorbing semiconductor and the electron donor/hole transporter, while PC<sub>61</sub>BM acted as the electron acceptor/transporter. To-date, the majority of solar cells featuring BODIPY polymers do not exceed a PCE of 3%,<sup>111–116</sup> with a few exceptions.<sup>77,117–120</sup> The ideal BODIPY polymers for solar cells should have a narrow energy gap for good solar absorption, high charge mobility, well-matched energy levels with the other heterojunction components to facilitate charge transfer, and precisely-controlled phase separation (on the order of the exciton diffusion length). To the point of broad solar absorption (~300-900 nm) Li and co-workers synthesized a thienylBODIPY-*alt*-thienyl benzodithiophene polymer, **P30**, and blended it with a non-fullerene small molecule acceptor to achieve a record PCE (for a BODIPY-based solar cells) of ~9.9% (Figure 17c).<sup>121</sup>

**Thin film transistors.** For the case of OTFTs, Thayumanavan and co-workers were the first to examine  $\pi$ -conjugated BODIPY

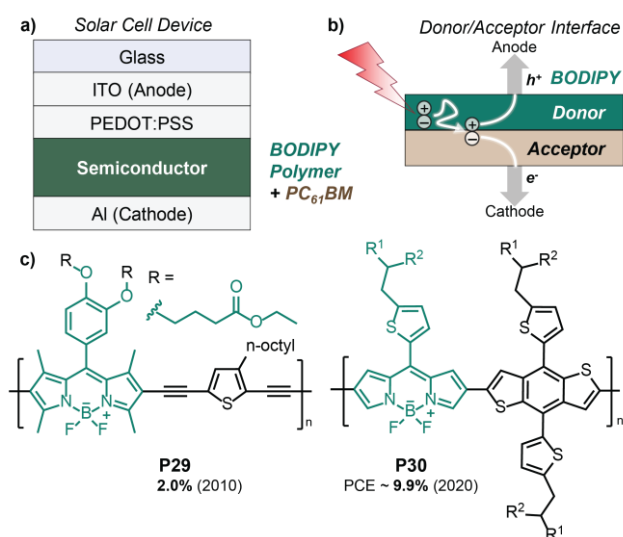


**Figure 17.** BODIPY polymers in solar cells. a) Cross-sectional device architecture. b) General schematic of charge generation and transfer. c) Chemical structures of the first BODIPY polymer, **P29**, and highest performance polymer to-date, **P30**, in solar cells. ITO = indium tin oxide, [6,6]-phenyl-C<sub>61</sub>-butyric acid methyl ester = PC<sub>61</sub>BM, PEDOT:PSS = poly(3,4-ethylenedioxythiophene) polystyrene sulfonate, Al = aluminium,  $h^+$  = hole,  $e^-$  = electron. Reproduced from ref. 110 and 121 with permission from the Royal Society of Chemistry, copyright 2011 and 2020.

polymers, however the charge transport mobility values measured were low, on the order of  $10^{-5}$  to  $10^{-6}$   $\text{cm}^2\text{V}^{-1}\text{S}^{-1}$ .<sup>84</sup> Subsequently, Facchetti, Stoddart, Usta, and co-workers examined a series of BODIPY D-A polymers in OTFTs, discovering a record-high hole mobility ( $\mu_h > 0.1$   $\text{cm}^2\text{V}^{-1}\text{S}^{-1}$ ) for a poly(BODIPY-*alt*-thiophene) derivative, **P31** (Figure 18).<sup>79</sup> Recent efforts have focused on the development of BODIPY polymers capable of transporting both holes and electrons (i.e., ambipolar transport), as this would enable a single, more sophisticated, device to have switchability between two mobile channels, as opposed to requiring two separate devices for this purpose. To this end, diketopyrrolopyrrole (DPP), a planar molecule containing a quadrupole (constructive superposition of two dipoles), was selected as a comonomer with BODIPY to afford **P32**, providing a balanced hole and electron mobility ( $\sim 0.01$   $\text{cm}^2\text{V}^{-1}\text{S}^{-1}$ ) (Figure 18c).<sup>122</sup>

**Chemosensors.** Because of its excellent photophysical properties, including high extinction coefficients and emission quantum yields, researchers have leveraged BODIPYs for chemical sensing applications. Although numerous examples exist for BODIPY-based fluorescent sensors,<sup>7</sup> the emphasis here is placed on the recent utility of BODIPY-based polymers. For example, Zhang and co-workers prepared water-soluble BODIPYs containing PEG chains and dithia-dioxa-aza cyclopentadecane crown ethers, **P33**.<sup>123</sup> In water **P33** was non-fluorescent due to intramolecular charge transfer (ICT). However, upon Hg<sup>2+</sup> capture ICT was shut down resulting in a distinct color change and increase in emission (Figure 19a). The derivatives had excellent selectivity for Hg<sup>2+</sup> relative to other metal cations, as well as high sensitivity, with a limit of detection down to 8.1 ppb (Figure 19b). In another report, Liu and co-workers synthesized a series of  $\pi$ -conjugated BODIPY polymer turn-off sensors, which were selective for fluoride and cyanide ions over other anions (e.g., Cl<sup>-</sup>, Br<sup>-</sup>, I<sup>-</sup>). The strong emission quenching by fluoride and cyanide ions was ascribed to a reaction at the boron center of BODIPY.

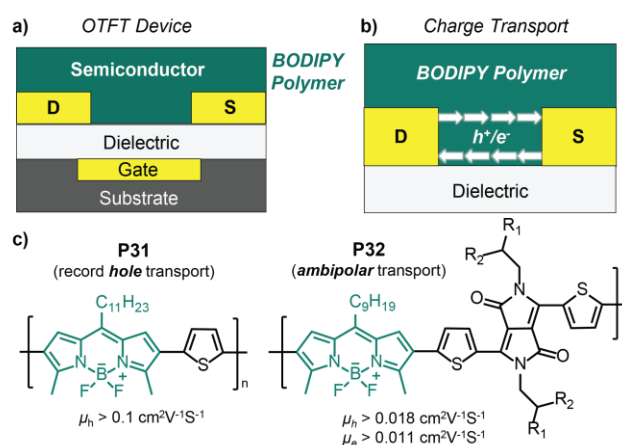


**Figure 18.** BODIPY polymers in organic thin film transistor (OTFT) devices. a) Cross-sectional device architecture. b) General schematic of charge transport. c) Chemical structures of BODIPY polymers for OTFT applications that have provided record hole, **P31**, and ambipolar (hole and electron), **P32**, transport.  $h^+$  = hole,  $e^-$  = electron, D = drain, S = source,  $\mu_h$  = hole transport,  $\mu_e$  = electron transport. Reproduced from ref. 79 with permission from Wiley-VCH, copyright 2013. Reproduced from ref. 122 with permission from American Chemical Society, copyright 2016.

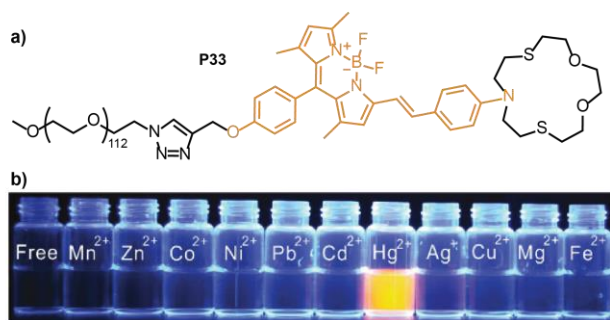


**Figure 19.** Example of a BODIPY-based polymer chemical sensor. a) Chemical structure of **P33**; b) Selective fluorescence turn-on sensing of  $\text{Hg}^{2+}$  over other metal cations in water. Reproduced from ref. 123 with permission from the Royal Society of Chemistry, copyright 2015.

**Heterogeneous photocatalysts.** BODIPY derivatives have also demonstrated utility as heterogeneous photocatalysts that benefit from access to triplet excited-states. For example, BODIPY derivatives have been employed for photooxidation via singlet oxygen ( $^1\text{O}_2$ ) generation. As mentioned previously,  $^1\text{O}_2$  occurs through a triplet-triplet (T-T) energy transfer between the triplet excited-state of BODIPY and oxygen. Thus, BODIPY derivatives capable of efficient intersystem crossing (ISC) to a triplet state are required. To this end, Jing and co-workers synthesized BODIPY-based porous heterogeneous photocatalysts.<sup>91</sup> By locking BODIPY molecules into a rigid polystyrene framework it is hypothesized that ISC to a triplet state was enhanced, which, coupled with a high surface area, resulted in good photocatalytic efficiency for oxidizing thioanisoles upon exposure to visible light ( $> 395$  nm). Following the same strategy, Liras and co-workers synthesized a BODIPY-based  $\pi$ -conjugated microporous polymer, **P34**, with a high surface area ( $299 \text{ m}^2 \text{ g}^{-1}$ ) (**Figure 20**).<sup>124</sup> Compared to the corresponding monomers, the microporous polymer was shown to be four times more efficient at oxidizing thioanisole to methylphenyl sulfoxide upon exposure to visible light ( $> 500$

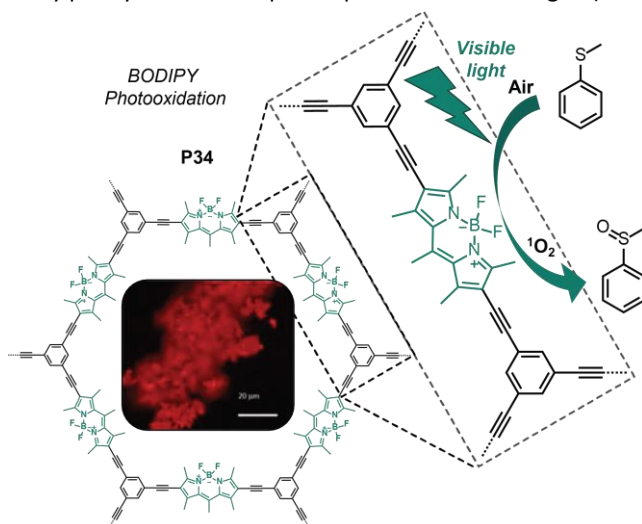


**Figure 20.** Chemical structure of a BODIPY-based porous photocatalyst, **P34**, along with the oxidation process of thioanisole upon exposure to  $> 500$  nm visible light. The central picture is fluorescence microscope image of the photocatalyst.  $^1\text{O}_2$  = singlet oxygen. Figure adapted with permission from reference 124. Copy right (2016) American Chemical Society.

nm). In a very recent paper, Hupp, Stoddart, Deria, and co-workers reported the preparation of halogenated BODIPY-based porous organic polymers through post-synthetic modification of the parent hydrogenated precursor.<sup>125</sup> Both brominated and iodinated derivatives served to accelerate the catalytic photo-oxidation of 2-chloroethyl ethyl sulfide to 2-chloroethyl ethyl sulfoxide by five-fold. These examples highlight the utility of BODIPYs in heterogeneous photocatalysis applications.

### 4.3 Emerging applications in polymer synthesis and degradation

**Photocages for (de)polymerization.** BODIPY photocages have been used in both the production and destruction of polymers upon irradiation. For example, Sebastián, Hernando and co-workers demonstrated photolysis of a carbamate functionalized BODIPY upon exposure to green light ( $\sim 532$  nm), followed by decarboxylation to release diethylamine to catalyze the anionic polymerization of cyanoacrylates.<sup>126</sup> Overall, the BODIPY photocages used in this study were stable in the dark and were able to provide the on-demand formation of polymers with excellent adhesive behaviour. The spatiotemporal control offered by this approach is attractive for utilizing cyanoacrylate polymerizations in future biomedical applications.

In a recent example, Truong and co-workers established a method for direct photorelease of thiol anions from BODIPY photocages upon exposure to green light ( $\sim 530$  nm).<sup>127</sup> The released thiolates reacted with propiolates through a Michael-type thiol-yne addition in water. Building on this chemistry, a tetrafunctional BODIPY photocage prepolymer, **P35**, was reacted with a tetrafunctional propiolate prepolymer, **P36**, to afford hydrogels upon irradiation with green light (**Figure 21**). The authors elegantly demonstrated the ability to spatially

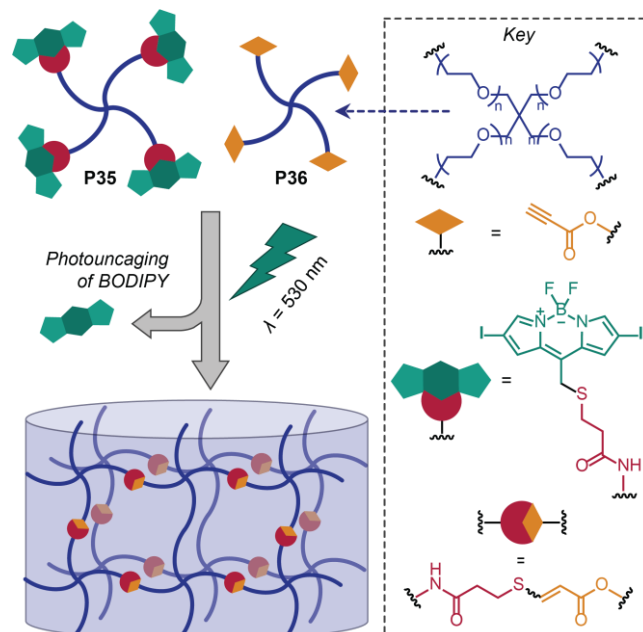


**Figure 21.** Schematic representation of hydrogel formation using a tetrafunctional BODIPY photocage prepolymer **P35** and tetrafunctional propiolate prepolymer **P36**. Irradiation with green light ( $\sim 530$  nm) results in direct release of thiolates that undergo a Michael-type thiol-yne addition in water. Figure adapted with permission from reference 127. Copy right (2019) Wiley-VCH.

pattern the hydrogel formation by irradiating through a photomask. The utility of visible light to activate a mild crosslinking reaction in the formation of hydrogels holds exciting promise for utility in the emerging field of bioprinting for regenerative medicine.

The degradation of polymers using BODIPY photocage chemistry presents a number of opportunities to take advantage of these versatile and efficient materials as little has been examined to-date. In one of the few examples, Ambade and co-workers demonstrated the degradation of micelles comprising poly(ethylene glycol-*b*-styrene) held together by a central BODIPY photocage, **P37** (Figure 22a).<sup>128</sup> Upon exposure to visible light (~470-490 nm) photolysis uniquely occurred at the B-O bond, resulting in micelle disassembly due to a loss of the hydrophilic-hydrophobic balance, as supported by transmission electron microscopy and the qualitative observation of polymer precipitation in water (likely the hydrophobic polystyrene fragment) after irradiation (Figure 22b).

**Photoredox polymerization.** The first report of utilizing BODIPY for photoredox polymerization was accomplished by Lalev e and co-workers, where both radical and cationic polymerizations were demonstrated.<sup>129</sup> Triggered by visible light centred at 473 nm, acrylate/vinyl ether blends could be cured to afford crosslinked interpenetrating polymer networks, that possessed two different glass transition temperatures (-11 and 111  C). Recently, the same group demonstrated that BODIPYs could be used in the photothermal polymerization of methacrylates with NIR light (785 nm and 940 nm).<sup>130</sup> Here, a thermal initiator was added to facilitate the polymerization, which was activated through a photothermal effect, wherein absorption of NIR light by BODIPY resulted in a non-radiative thermal relaxation event (release of heat). However, due to the low molar absorptivity of the selected BODIPY derivatives at those wavelengths high intensity NIR lasers were required (~400-4000 mW/cm<sup>2</sup>).

To further increase the efficiency of BODIPY photoredox polymerizations, our group carried out a systematic investigation on a small library of dyes, demonstrating the effect of halogenation under identical photon absorption conditions (Figure 23a).<sup>131</sup> As noted previously, halogenation

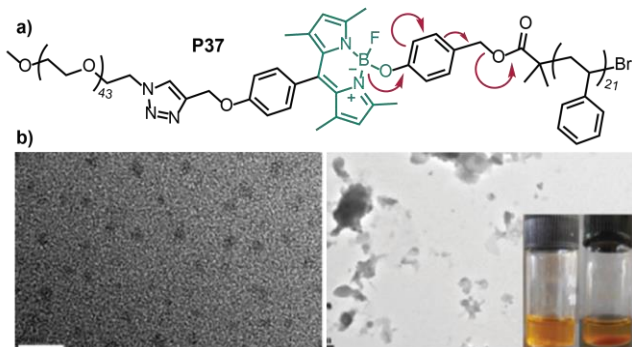


**Figure 22.** Photo-degradation of poly(ethylene glycol-*b*-styrene) connected in the center through a BODIPY photocage. a) Chemical structure of block copolymer **P37**; b) TEM images for 0.1 wt% aqueous solution of **P37** before (left) and after (right) irradiation, showing disassembly upon photolysis. Inset: photographs of polymer solution before (left) and after (right) irradiation. Reproduced from ref. 128 with permission from the Royal Society of Chemistry, copyright 2015.

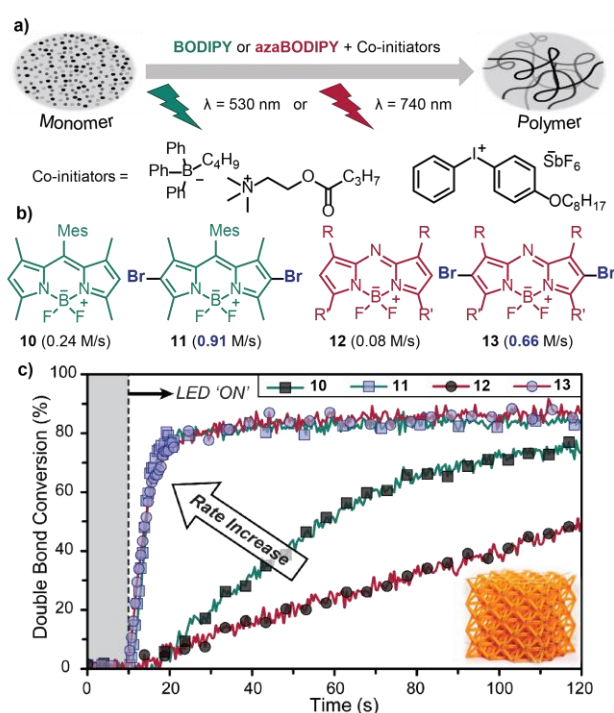


**Figure 23.** Effect of halogenation on BODIPYs as photoredox catalysts for free radical polymerization. a) Schematic representation of the polymerization and its components. b) Chemical structures of BODIPYs and azaBODIPYs, and corresponding photopolymerization rates using an equivalent number of photons absorbed. c) Overlay of double bond conversion (monomer consumption) vs. time for (aza)BODIPYs **10-13**. Inset shows a digital image of a complex lattice structure 3D printed with low energy green light (~530 nm, ~2 mW/cm<sup>2</sup>) using BODIPY. Scale bar represents 5 mm. Figure adapted with permission from reference 131. Copy right (2020) American Chemical Society.

(e.g., Br or I) of the BODIPY framework dramatically enhances ISC rates, resulting in a larger population of long-lived triplet excited states. As such, more collisions occur per photon absorbed, increasing the probability of a successful electron/energy transfer event to occur between BODIPY and a co-initiator to initiate polymerization. Excitingly the halogenated BODIPY, **11**, resulted in a 4× polymerization rate enhancement relative to the non-halogenated analogue, **10** (Figure 23b). Moreover an 8× rate increase was observed for the halogenated azaBODIPY, **13**, relative to the non-halogenated azaBODIPY, **12**, providing unprecedented photocuring rates (< 1 min to final monomer conversion) with far-red ( $\lambda_{ex}^{max} = 740$  nm) light at an ultralow intensity (1.0 mW/cm<sup>2</sup>) or catalyst loading (0.004 mol%) (Figure 23c). The efficient polymerization enabled the utility of BODIPY photoredox catalysts in rapid high-resolution visible light-based 3D printing, as shown with the inset image of a lattice structure in Figure 23c.

## 5. Summary and Future Outlook

To summarize, BODIPYs represent an incredibly versatile class of compounds that, when combined with polymeric materials, have cutting-edge applications in biomedicine, optoelectronics, chemosensors, and photocatalysis. Furthermore, these BODIPYs are emerging as promising components to efficiently

initiate polymerizations using low energy visible-to-NIR light. The broad applicability of BODIPYs stems from their synthetically tunable scaffold, which offers fine control over their properties and reactivity, including absorption wavelength and strength, emission wavelength and yield, reduction and oxidation potentials, excited state lifetime and triplet yield, and bond photolysis. Although significant research efforts and discoveries have been made surrounding BODIPYs, there remains valuable untapped potential, as evidenced by discoveries published in the last year.<sup>51,108,125,127,131–138</sup>

To provoke further thought in considering the future of BODIPYs in polymer chemistry, we describe five potential directions (in no particular order) to be explored that will enable next generation materials and applications:

- (i) *Identifying more efficient and red-shifted photocages for (de)polymerization;*
- (ii) *Preparing near infrared (>780 nm) (water soluble) derivatives with high triplet yields;*
- (iii) *Understanding the structure-property limitations of light driven electron/energy transfer;*
- (iv) *Developing wavelength-selective photoredox chemistry for multi-material fabrication; and*
- (v) *Leveraging photon upconversion to drive high energy polymer chemistry with low energy and intensity light.*

Examining current BODIPYs systematically, while continuing to expand their scope to identify those that strongly and narrowly absorb far-red/NIR light, generate long lived triplet excited states poised for upconversion processes, and/or demonstrate improved water solubility will enable use in applications requiring a mild and low energy input at minimal (catalytic) material costs. In particular, the sharp absorption bands of BODIPY derivatives make them excellent candidates for the development of wavelength-specific chemistry, which has potential utility in additive manufacturing to access multi-functional/material objects with spatiotemporally coded composition and properties. Furthermore, when BODIPY derivatives with 1) superior water solubility and 2) high molar absorptivity in the NIR are obtained, they will serve as powerful curing agents for emergent biomedical applications, such as bioprinting. To realize the aforementioned advancements will require a deep understanding of structure-property relationships, and a strong collaboration between computational and experimental chemists will undoubtedly accelerate these efforts. The future of BODIPYs in polymer chemistry is surely bright!

## Conflicts of interest

There are no conflicts to declare.

## Acknowledgements

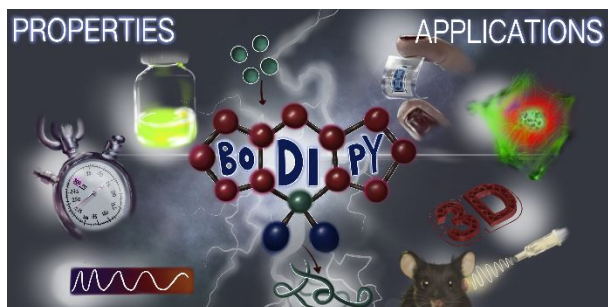
We thank the Robert A. Welch Foundation (F-2007) and the Center for Dynamics and Control of Materials: an NSF MRSEC (DMR-1720595) for financial support.

## Notes and references

- 1 A. Treibs and F.-H. Kreuzer, *Justus Liebigs Ann. Chem.*, 1968, **718**, 208–223.
- 2 A. Loudet and K. Burgess, *Chem. Rev.*, 2007, **107**, 4891–4932.
- 3 M. Benstead, G. H. Mehl and R. W. Boyle, *Tetrahedron*, 2011, **67**, 3573–3601.
- 4 A. Kamkaew, S. H. Lim, H. B. Lee, L. V. Kiew, L. Y. Chung and K. Burgess, *Chem Soc Rev*, 2013, **42**, 77–88.
- 5 J. Bañuelos, *Chem. Rec.*, 2016, **16**, 335–348.
- 6 N. Boens, V. Leen and W. Dehaen, *Chem Soc Rev*, 2012, **41**, 1130–1172.
- 7 T. Kowada, H. Maeda and K. Kikuchi, *Chem. Soc. Rev.*, 2015, **44**, 4953–4972.
- 8 Y. Ge and D. F. O'Shea, *Chem. Soc. Rev.*, 2016, **45**, 3846–3864.
- 9 D. Ho, R. Ozdemir, H. Kim, T. Earmme, H. Usta and C. Kim, *ChemPlusChem*, 2018, cplu.201800543.
- 10 A. Bessette and G. S. Hanan, *Chem Soc Rev*, 2014, **43**, 3342–3405.
- 11 H. Klfout, A. Stewart, M. Elkhalfa and H. He, *ACS Appl. Mater. Interfaces*, 2017, **9**, 39873–39889.
- 12 M. L. Agazzi, M. B. Ballatore, A. M. Durantini, E. N. Durantini and A. C. Tomé, *J. Photochem. Photobiol. C Photochem. Rev.*, 2019, **40**, 21–48.
- 13 A. Turksoy, D. Yildiz and E. U. Akkaya, *Coord. Chem. Rev.*, 2019, **379**, 47–64.
- 14 R. Ziessel, G. Ulrich and A. Harriman, *New J. Chem.*, 2007, **31**, 496.
- 15 G. Ulrich, R. Ziessel and A. Harriman, *Angew. Chem. Int. Ed.*, 2008, **47**, 1184–1201.
- 16 H. Staudinger, *Berichte Dtsch. Chem. Ges. B Ser.*, 1920, **53**, 1073–1085.
- 17 H. Frey and T. Johann, *Polym. Chem.*, 2020, **11**, 8–14.
- 18 Y. Liang, L. Li, R. A. Scott and K. L. Kiick, *Macromolecules*, 2017, **50**, 483–502.
- 19 S. K. Kumar, B. C. Benicewicz, R. A. Vaia and K. I. Winey, *Macromolecules*, 2017, **50**, 714–731.
- 20 D. K. Schneiderman and M. A. Hillmyer, *Macromolecules*, 2017, **50**, 3733–3749.
- 21 J. H. Park and G. C. Rutledge, *Macromolecules*, 2017, **50**, 5627–5642.
- 22 M. Galizia, W. S. Chi, Z. P. Smith, T. C. Merkel, R. W. Baker and B. D. Freeman, *Macromolecules*, 2017, **50**, 7809–7843.
- 23 N. Boens, B. Verbelen, M. J. Ortiz, L. Jiao and W. Dehaen, *Coord. Chem. Rev.*, 2019, **399**, 213024.
- 24 G. Fan, L. Yang and Z. Chen, *Front. Chem. Sci. Eng.*, 2014, **8**, 405–417.
- 25 L. Jean-Gérard, W. Vasseur, F. Scherninski and B. Andrioletti, *Chem. Commun.*, 2018, **54**, 12914–12929.
- 26 V. Lakshmi, M. Rajeswara Rao and M. Ravikanth, *Org. Biomol. Chem.*, 2015, **13**, 2501–2517.
- 27 Z. Dost, S. Atilgan and E. U. Akkaya, *Tetrahedron*, 2006, **62**, 8484–8488.
- 28 O. Buyukcakir, O. A. Bozdemir, S. Kolemen, S. Erbas and E. U. Akkaya, *Org. Lett.*, 2009, **11**, 4644–4647.
- 29 M. Laine, N. A. Barbosa, R. Wieczorek, M. Ya. Melnikov and A. Filarowski, *J. Mol. Model.*, 2016, **22**, 260.

- 30 C. Goze, G. Ulrich, L. J. Mallon, B. D. Allen, A. Harriman and R. Ziessel, *J. Am. Chem. Soc.*, 2006, **128**, 10231–10239.
- 31 G. Ulrich, C. Goze, M. Guardigli, A. Roda and R. Ziessel, *Angew. Chem. Int. Ed.*, 2005, **44**, 3694–3698.
- 32 A. Harriman, G. Izzet and R. Ziessel, *J. Am. Chem. Soc.*, 2006, **128**, 10868–10875.
- 33 N. J. Turro, V. Ramamurthy and J. C. Scaiano, *Modern molecular photochemistry of organic molecules*, University Science Books, Sausalito, Calif, 2010.
- 34 I. J. Arroyo, R. Hu, G. Merino, B. Z. Tang and E. Peña-Cabrera, *J. Org. Chem.*, 2009, **74**, 5719–5722.
- 35 I. Esnal, I. Valois-Escamilla, C. F. A. Gómez-Durán, A. Urías-Benavides, M. L. Betancourt-Mendiola, I. López-Arbeloa, J. Bañuelos, I. García-Moreno, A. Costela and E. Peña-Cabrera, *ChemPhysChem*, 2013, **14**, 4134–4142.
- 36 K. Krumova and G. Cosa, *J. Am. Chem. Soc.*, 2010, **132**, 17560–17569.
- 37 R. Lincoln, L. E. Greene, K. Krumova, Z. Ding and G. Cosa, *J. Phys. Chem. A*, 2014, **118**, 10622–10630.
- 38 X.-F. Zhang, X. Yang, K. Niu and H. Geng, *J. Photochem. Photobiol. Chem.*, 2014, **285**, 16–20.
- 39 J. Zhao, K. Xu, W. Yang, Z. Wang and F. Zhong, *Chem. Soc. Rev.*, 2015, **44**, 8904–8939.
- 40 J. Zhao, W. Wu, J. Sun and S. Guo, *Chem. Soc. Rev.*, 2013, **42**, 5323.
- 41 C. S. Kue, S. Y. Ng, S. H. Voon, A. Kamkaew, L. Y. Chung, L. V. Kiew and H. B. Lee, *Photochem. Photobiol. Sci.*, 2018, **17**, 1691–1708.
- 42 M. Gorbe, A. M. Costero, F. Sancenón, R. Martínez-Mañez, R. Ballesteros-Cillero, L. E. Ochando, K. Chulvi, R. Gotor and S. Gil, *Dyes Pigments*, 2019, **160**, 198–207.
- 43 A. Gorman, J. Killoran, C. O'Shea, T. Kenna, W. M. Gallagher and D. F. O'Shea, *J. Am. Chem. Soc.*, 2004, **126**, 10619–10631.
- 44 P. Klán, T. Šolomek, C. G. Bochet, A. Blanc, R. Givens, M. Rubina, V. Popik, A. Kostikov and J. Wirz, *Chem. Rev.*, 2013, **113**, 119–191.
- 45 T. Šolomek, J. Wirz and P. Klán, *Acc. Chem. Res.*, 2015, **48**, 3064–3072.
- 46 E. Palao, T. Slanina, L. Muchová, T. Šolomek, L. Vítek and P. Klán, *J. Am. Chem. Soc.*, 2016, **138**, 126–133.
- 47 D. Kand, L. Pizarro, I. Angel, A. Avni, D. Friedmann-Morvinski and R. Weinstain, *Angew. Chem. Int. Ed.*, 2019, **58**, 4659–4663.
- 48 J. A. Peterson, L. J. Fischer, E. J. Gehrman, P. Shrestha, D. Yuan, C. S. Wijesooriya, E. A. Smith and A. H. Winter, *J. Org. Chem.*, 2020, **85**, 5712–5717.
- 49 T. Slanina, P. Shrestha, E. Palao, D. Kand, J. A. Peterson, A. S. Dutton, N. Rubinstein, R. Weinstain, A. H. Winter and P. Klán, *J. Am. Chem. Soc.*, 2017, **139**, 15168–15175.
- 50 J. A. Peterson, C. Wijesooriya, E. J. Gehrman, K. M. Mahoney, P. Goswami, T. R. Albright, A. Syed, A. S. Dutton, E. A. Smith and A. H. Winter, *J. Am. Chem. Soc.*, 2018, **140**, 7343–7346.
- 51 P. Shrestha, K. C. Dissanayake, E. J. Gehrman, C. S. Wijesooriya, A. Mukhopadhyay, E. A. Smith and A. H. Winter, *J. Am. Chem. Soc.*, 2020, **142**, 15505–15512.
- 52 N. Umeda, H. Takahashi, M. Kamiya, T. Ueno, T. Komatsu, T. Terai, K. Hanaoka, T. Nagano and Y. Urano, *ACS Chem. Biol.*, 2014, **9**, 2242–2246.
- 53 K. Sambath, T. Zhao, Z. Wan and Y. Zhang, *Chem. Commun.*, 2019, **55**, 14162–14165.
- 54 D. McCoul, W. Hu, M. Gao, V. Mehta and Q. Pei, *Adv. Electron. Mater.*, 2016, **2**, 1500407.
- 55 J. Kim, M.-S. Lee, S. Jeon, M. Kim, S. Kim, K. Kim, F. Bien, S. Y. Hong and J.-U. Park, *Adv. Mater.*, 2015, **27**, 3292–3297.
- 56 Z. Li, C.-C. Chueh and A. K.-Y. Jen, *Prog. Polym. Sci.*, 2019, **99**, 101175.
- 57 Z. Zeng, Z. Zhong, W. Zhong, J. Zhang, L. Ying, G. Yu, F. Huang and Y. Cao, *J. Mater. Chem. C*, 2019, **7**, 6070–6076.
- 58 A. M. Pappa, D. Ohayon, A. Giovannitti, I. P. Maria, A. Savva, I. Uguz, J. Rivnay, I. McCulloch, R. M. Owens and S. Inal, *Sci. Adv.*, 2018, **4**, eaat0911.
- 59 B. M. Squeo, V. G. Gregoriou, A. Avgeropoulos, S. Baysec, S. Allard, U. Scherf and C. L. Chochos, *Prog. Polym. Sci.*, 2017, **71**, 26–52.
- 60 J. Roncali, *Chem. Rev.*, 1992, **92**, 711–738.
- 61 G. Sabouraud, S. Sadki and N. Brodie, *Chem. Soc. Rev.*, 2000, **29**, 283–293.
- 62 F. Algi and A. Cihaner, *Polymer*, 2012, **53**, 3469–3475.
- 63 J. E. Dick, A. Poirel, R. Ziessel and A. J. Bard, *Electrochimica Acta*, 2015, **178**, 234–239.
- 64 M. D. Yilmaz, T. Aytun, M. Frascioni, S. I. Stupp and J. F. Stoddart, *Synth. Met.*, 2014, **197**, 52–57.
- 65 N. Miyaura, *J. Organomet. Chem.*, 2002, **653**, 54–57.
- 66 E. Negishi, *J. Organomet. Chem.*, 2002, **653**, 34–40.
- 67 A. Suzuki, *J. Organomet. Chem.*, 2002, **653**, 83–90.
- 68 K. Sonogashira, *J. Organomet. Chem.*, 2002, **653**, 46–49.
- 69 F. E. Alemдарoglu, S. C. Alexander, D. Ji, D. K. Prusty, M. Börsch and A. Herrmann, *Macromolecules*, 2009, **42**, 6529–6536.
- 70 V. R. Donuru, G. K. Vegesna, S. Velayudham, S. Green and H. Liu, *Chem. Mater.*, 2009, **21**, 2130–2138.
- 71 H. Yeo, K. Tanaka and Y. Chujo, *Macromolecules*, 2013, **46**, 2599–2605.
- 72 C. P. Sen, V. Devendar Goud, R. G. Shrestha, L. K. Shrestha, K. Ariga and S. Valiyaveetil, *Polym. Chem.*, 2016, **7**, 4213–4225.
- 73 A. Nagai, J. Miyake, K. Kokado, Y. Nagata and Y. Chujo, *J. Am. Chem. Soc.*, 2008, **130**, 15276–15278.
- 74 A. Cihaner and F. Algi, *Electrochimica Acta*, 2008, **54**, 786–792.
- 75 A. Nagai and Y. Chujo, *Macromolecules*, 2010, **43**, 193–200.
- 76 R. Yoshii, H. Yamane, A. Nagai, K. Tanaka, H. Taka, H. Kita and Y. Chujo, *Macromolecules*, 2014, **47**, 2316–2323.
- 77 M. Kyeong, J. Lee, K. Lee and S. Hong, *ACS Appl. Mater. Interfaces*, 2018, **10**, 23254–23262.
- 78 G. Meng, S. Velayudham, A. Smith, R. Luck and H. Liu, *Macromolecules*, 2009, **42**, 1995–2001.
- 79 H. Usta, M. D. Yilmaz, A.-J. Avestro, D. Boudinet, M. Denti, W. Zhao, J. F. Stoddart and A. Facchetti, *Adv. Mater.*, 2013, **25**, 4327–4334.
- 80 C. Thivierge, A. Loudet and K. Burgess, *Macromolecules*, 2011, **44**, 4012–4015.
- 81 R. Yoshii, A. Nagai, K. Tanaka and Y. Chujo, *J. Polym. Sci. Part Polym. Chem.*, 2013, **51**, 1726–1733.
- 82 J. Roncali, *Chem. Rev.*, 1997, **97**, 173–206.
- 83 Z. Zhang and J. Wang, *J. Mater. Chem.*, 2012, **22**, 4178.
- 84 B. C. Popere, A. M. Della Pelle and S. Thayumanavan, *Macromolecules*, 2011, **44**, 4767–4776.
- 85 B. C. Popere, A. M. Della Pelle, A. Poe, G. Balaji and S. Thayumanavan, *Chem. Sci.*, 2012, **3**, 3093.
- 86 B. M. Squeo, V. G. Gregoriou, Y. Han, A. Palma-Cando, S. Allard, E. Serpetzoglou, I. Konidakis, E. Stratakis, A. Avgeropoulos, T. D. Anthopoulos, M. Heaney, U. Scherf and C. L. Chochos, *J. Mater. Chem. C*, 2018, **6**, 4030–4040.
- 87 Y. Wang, Y. Zhang, W. Hu, Y. Quan, Y. Li and Y. Cheng, *ACS Appl. Mater. Interfaces*, 2019, **11**, 26165–26173.
- 88 Y. Wang, Y. Li, S. Liu, F. Li, C. Zhu, S. Li and Y. Cheng, *Macromolecules*, 2016, **49**, 5444–5451.

- 89 J. Chen, W. Zhong, Y. Tang, Z. Wu, Y. Li, P. Yi and J. Jiang, *Macromolecules*, 2015, **48**, 3500–3508.
- 90 R. Sauer, A. Turshatov, S. Balushev and K. Landfester, *Macromolecules*, 2012, **45**, 3787–3796.
- 91 W. Li, W. Zhang, X. Dong, L. Yan, R. Qi, W. Wang, Z. Xie and X. Jing, *J. Mater. Chem.*, 2012, **22**, 17445.
- 92 F. Marsico, A. Turshatov, K. Weber and F. R. Wurm, *Org. Lett.*, 2013, **15**, 3844–3847.
- 93 D. A. Hinton, J. D. Ng, J. Sun, S. Lee, S. K. Saikin, J. Logsdon, D. S. White, A. N. Marquard, A. C. Cavell, V. K. Krasecki, K. A. Knapper, K. M. Lupo, M. R. Wasielewski, A. Aspuru-Guzik, J. S. Biteen, P. Gopalan and R. H. Goldsmith, *J. Am. Chem. Soc.*, 2018, **140**, 15827–15841.
- 94 S. Kaga, S. Yapar, E. M. Gecici and R. Sanyal, *Macromolecules*, 2015, **48**, 5106–5115.
- 95 M. Liras, J. M. García-García, I. Quijada-Garrido, A. Gallardo and R. París, *Macromolecules*, 2011, **44**, 3739–3745.
- 96 I. Kosif, E.-J. Park, R. Sanyal and A. Sanyal, *Macromolecules*, 2010, **43**, 4140–4148.
- 97 Y. N. Yuksekdog, T. N. Gevrek and A. Sanyal, *ACS Macro Lett.*, 2017, **6**, 415–420.
- 98 D. Schaeffel, S. Yordanov, R. H. Staff, A. Kreyes, Y. Zhao, M. Schmidt, K. Landfester, J. Hofkens, H.-J. Butt, D. Crespy and K. Koynov, *ACS Macro Lett.*, 2015, **4**, 171–176.
- 99 C. Grazon, J. Rieger, R. Méallet-Renault, B. Charleux and G. Clavier, *Macromolecules*, 2013, **46**, 5167–5176.
- 100C. Grazon, J. Rieger, B. Charleux, G. Clavier and R. Méallet-Renault, *J. Phys. Chem. C*, 2014, **118**, 13945–13952.
- 101C. Grazon, J. Rieger, P. Beaunier, R. Méallet-Renault and G. Clavier, *Polym. Chem.*, 2016, **7**, 4272–4283.
- 102R. París, I. Quijada-Garrido, O. García and M. Liras, *Macromolecules*, 2011, **44**, 80–86.
- 103Z. M. Hudson, D. J. Lunn, M. A. Winnik and I. Manners, *Nat. Commun.*, 2014, **5**, 3372.
- 104H. Qiu, Y. Gao, C. E. Boott, O. E. C. Gould, R. L. Harniman, M. J. Miles, S. E. D. Webb, M. A. Winnik and I. Manners, *Science*, 2016, **352**, 697–701.
- 105C. Wu and D. T. Chiu, *Angew. Chem. Int. Ed.*, 2013, **52**, 3086–3109.
- 106L. Chen, D. Chen, Y. Jiang, J. Zhang, J. Yu, C. C. DuFort, S. R. Hingorani, X. Zhang, C. Wu and D. T. Chiu, *Angew. Chem. Int. Ed.*, 2019, **58**, 7008–7012.
- 107C. Tian, J. Niu, X. Wei, Y. Xu, L. Zhang, Z. Cheng and X. Zhu, *Nanoscale*, 2018, **10**, 10277–10287.
- 108S. Qi, N. Kwon, Y. Yim, V.-N. Nguyen and J. Yoon, *Chem. Sci.*, 2020, **11**, 6479–6484.
- 109L. Huang, Z. Li, Y. Zhao, Y. Zhang, S. Wu, J. Zhao and G. Han, *J. Am. Chem. Soc.*, 2016, **138**, 14586–14591.
- 110B. Kim, B. Ma, V. R. Donuru, H. Liu and J. M. J. Fréchet, *Chem. Commun.*, 2010, **46**, 4148.
- 111D. Cortizo-Lacalle, C. T. Howells, S. Gambino, F. Vilela, Z. Vobecka, N. J. Findlay, A. R. Inigo, S. A. J. Thomson, P. J. Skabara and I. D. W. Samuel, *J. Mater. Chem.*, 2012, **22**, 14119.
- 112G. Tarafdar, U. K. Pandey, S. Sengupta and P. C. Ramamurthy, *Sol. Energy*, 2019, **186**, 215–224.
- 113S. P. Economopoulos, C. L. Chochos, H. A. Ioannidou, M. Neophytou, C. Charilaou, G. A. Zissimou, J. M. Frost, T. Sachetan, M. Shahid, J. Nelson, M. Heeney, D. D. C. Bradley, G. Itskos, P. A. Koutentis and S. A. Choulis, *RSC Adv.*, 2013, **3**, 10221.
- 114A. He, Y. Qin, W. Dai and X. Luo, *Dyes Pigments*, 2019, **162**, 671–679.
- 115W. He, Y. Jiang and Y. Qin, *Polym Chem*, 2014, **5**, 1298–1304.
- 116B. M. Squeo, N. Gasparini, T. Ameri, A. Palma-Cando, S. Allard, V. G. Gregoriou, C. J. Brabec, U. Scherf and C. L. Chochos, *J. Mater. Chem. A*, 2015, **3**, 16279–16286.
- 117L. Bucher, N. Desbois, P. D. Harvey, C. P. Gros, R. Misra and G. D. Sharma, *ACS Appl. Energy Mater.*, 2018, **1**, 3359–3368.
- 118L. Bucher, N. Desbois, P. D. Harvey, C. P. Gros and G. D. Sharma, *ACS Appl. Mater. Interfaces*, 2018, **10**, 992–1004.
- 119M. Ozdemir, S. W. Kim, H. Kim, M.-G. Kim, B. J. Kim, C. Kim and H. Usta, *Adv. Electron. Mater.*, 2018, **4**, 1700354.
- 120Y. Guo, D. Xia, B. Liu, H. Wu, C. Li, Z. Tang, C. Xiao and W. Li, *Macromolecules*, 2019, **52**, 8367–8373.
- 121B. Liu, Z. Ma, Y. Xu, Y. Guo, F. Yang, D. Xia, C. Li, Z. Tang and W. Li, *J. Mater. Chem. C*, 2020, **8**, 2232–2237.
- 122S. Singh, S. Chithiravel and K. Krishnamoorthy, *J. Phys. Chem. C*, 2016, **120**, 26199–26205.
- 123B. Wu, L. Xu, S. Wang, Y. Wang and W. Zhang, *Polym. Chem.*, 2015, **6**, 4279–4289.
- 124M. Liras, M. Iglesias and F. Sánchez, *Macromolecules*, 2016, **49**, 1666–1673.
- 125A. Atilgan, M. M. Cetin, J. Yu, Y. Beldjoudi, J. Liu, C. L. Stern, F. M. Cetin, T. Islamoglu, O. K. Farha, P. Deria, J. F. Stoddart and J. T. Hupp, *J. Am. Chem. Soc.*, 2020, jacs.0c07784.
- 126E. Faggi, J. Aguilera, R. Sáez, F. Pujol, J. Marquet, J. Hernando and R. M. Sebastián, *Macromolecules*, 2019, **52**, 2329–2339.
- 127M. Li, A. P. Dove and V. X. Truong, *Angew. Chem. Int. Ed.*, 2020, **59**, 2284–2288.
- 128N. G. Patil, N. B. Basutkar and A. V. Ambade, *Chem. Commun.*, 2015, **51**, 17708–17711.
- 129S. Telitel, J. Lalevée, N. Blanchard, T. Kavalli, M.-A. Tehfe, S. Schweizer, F. Morlet-Savary, B. Graff and J.-P. Fouassier, *Macromolecules*, 2012, **45**, 6864–6868.
- 130A. Bonardi, F. Bonardi, G. Noirbent, F. Dumur, C. Dietlin, D. Gimes, J.-P. Fouassier and J. Lalevée, *Polym. Chem.*, 2019, **10**, 6505–6514.
- 131A. Stafford, D. Ahn, E. K. Raulerson, K.-Y. Chung, K. Sun, D. M. Cadena, E. M. Forrister, S. R. Yost, S. T. Roberts and Z. A. Page, *J. Am. Chem. Soc.*, 2020, **142**, 14733–14742.
- 132J. A. Peterson, D. Yuan and A. Winter, *Multiwavelength Control of Mixtures Using Visible Light Absorbing Photocages*, 2020.
- 133K. Sitkowska, M. F. Hoes, M. M. Lerch, L. N. Lameijer, P. van der Meer, W. Szymański and B. L. Feringa, *Chem. Commun.*, 2020, **56**, 5480–5483.
- 134D. Kand, P. Liu, M. X. Navarro, L. J. Fischer, L. Rousso-Noori, D. Friedmann-Morvinski, A. H. Winter, E. W. Miller and R. Weinstein, *J. Am. Chem. Soc.*, 2020, **142**, 4970–4974.
- 135Z. Liu, J. Liu, Z. Zhang, Z. Sun, X. Shao, J. Guo, L. Xi, Z. Yuan, X. Zhang, D. T. Chiu and C. Wu, *Nanoscale*, 2020, **12**, 7522–7526.
- 136W. Zhang, W. Lin, C. Li, S. Liu, X. Hu and Z. Xie, *ACS Appl. Mater. Interfaces*, 2019, **11**, 32720–32728.
- 137K. Sambath, Z. Wan, Q. Wang, H. Chen and Y. Zhang, *Org. Lett.*, 2020, **22**, 1208–1212.
- 138Z. Wang, L. Huang, Y. Yan, A. M. El-Zohry, A. Toffoletti, J. Zhao, A. Barbon, B. Dick, O. F. Mohammed and G. Han, *Angew. Chem. Int. Ed.*, 2020, anie.202005269.



TOC sentence: The present review provides both a summary and outlook on the exciting field of BODIPYs in polymer chemistry.